UNIVERSITY OF CALIFORNIA, SAN DIEGO

Structural studies of TGF-beta superfamily members involved in the development of the musculoskeletal system

A Dissertation submitted in partial satisfaction of the

Requirements for the degree Doctor of Philosophy

in

Biology

by

Luis R. Esquivies

Committee in charge:

Professor Senyon Choe, Chair
Professor Russell Doolittle, Co-Chair
Professor Judy Kim
Professor Hector Viadiu
Professor Deborah Yelon

2013

The Dissertation of Luis R. Esquivies is approved, and it is acceptable in quality and form for publication on microfilm and electronically:

_____

_____

_____

_____

Co-chair

_____

Chair

University of California, San Diego

2013

DEDICATION

In dedication to my family, friends, and everyone who has made this journey possible.

EPIGRAPH

If I have seen further it is by standing on the shoulders of giants.

Sir Isaac Newton

TABLE OF CONTENTS

LIST OF FIGURES

LIST OF TABLES

ACKNOWLEDGEMENTS

I would like to thank my family for their support throughout my studies. In particular, I'd like to thank my parents Luis and Eva Patricia, for encouraging me to pursue my dreams, no matter how farfetched they may have been. I'd also like to thank my brother Carlos Cesar and my sister Eva Fernanda for their support.

I would also like to thank Dr. Senyon Choe for giving me the opportunity to embark on this journey. His unwavering support and optimism has been greatly appreciated. Furthermore, I'd like to thank Witek Kwiatkwoski, whose advice and support have proven invaluable. I'd also like to thank my doctoral committee members for giving me the opportunity to present my work to them.

Finally, I'd like to thank all members of the SBL-C lab, past and present, especially PEAL members Georgia Kefala, Katie Blain, Alissa Blackler, Michael Isaacs, Mark Vega, and George Allendorph. Their camaraderie and advice was always appreciated.

Chapter 2 is currently being prepared for submission for publication of the material. Esquivies L, Blackler A, Peran M, Rodriguez-Esteban C, Izpisua Belmonte C, Gray P, Booker E, Ahn C, Kwiatkowski W, Choe S. "Designer Nodal/BMP2 chimeras mimic Nodal signaling, promote chondrogenesis, and reveal a BMP2-like structure". The dissertation author was the primary investigator and author of this paper.

Chapter 3, in part is currently being prepared for submission for publication of the material. Yoon BH, Esquivies L, Ahn C, Ye SK, Kwiatkowski

W, Choe S. “A Noggin-insensitive Activin/BMP2 chimera, AB204, strongly accelerates osteogenic differentiation of preosteoblastic MC3T3-E1 cells and heals non-union bone defects in mice”. The dissertation author was a co-author of this paper.

VITA

Education

May 2005	Bachelor of Science in Biology, Emphasis on Cell and Molecular Biology, San Diego State University
September 2013	Doctor of Philosophy in Biology, University of California, San Diego

ABSTRACT OF THE DISSERTATION

Structural studies of TGF-beta superfamily members involved in the development of the musculoskeletal system

by

Luis R. Esquivies

Doctor of Philosophy in Biology

University of California, San Diego, 2013

Professor Senyon Choe, Chair
Professor Russell Doolittle, Co-Chair

The TGF-beta superfamily of proteins plays a crucial role in development. Given their wide-range of activities, the understanding of how these ligands are able to elicit such diverse biological responses using a very limited number of receptors is paramount. Structural studies have provided valuable insight into how some of these ligands function, however there still

remains many ligands that have not been able to be studied given their difficulty to be produced in quantities suitable for structural as well as functional analysis.

The focus of this work is on TGF-β ligands that play a role in the development of the musculoskeletal system. Using a novel technique termed Random Assembly of Heteromer Chimeras, or RASCH, functionally equivalent ligands of TGF-β ligands Nodal and Activin, two ligands involved in chondrogenic and osteogenic signaling pathways, have been produced, and their structures solved. This technique has also yielded chimeras with novel properties, such as enhanced osteogenesis. The structure of one such chimera, termed AB204, is presented. Additionally, structures of two members of another subset of the BMP ligands, GDF6 and GDF7, both involved in tenogenic signaling, were solved. In addition to the structures presented, mechanistic models that explain how these ligands assemble their signaling complexes are presented based on the information obtained from these structures.

Chapter 1. Introduction

The TGF-β Superfamily of Ligands

The Transforming Growth Factor β superfamily of proteins plays a crucial role in the development of both vertebrate and invertebrate organisms, their importance highlighted by the fact that orthologs of these proteins can be found in some of the most primitive metazoans (1).

The TGF-β superfamily of ligands is comprised of 33 members in the human genome (2), and can be divided into 2 subfamilies based on sequence similarity and the signaling pathways they activate: TGF-β/Activin/Nodal and BMP/GDF/MIS (3).

TGF-β ligands are expressed as inactive precursor molecules with a large N-terminal pro domain approximately 50-30 KDa in size that is sequentially cleaved in order to activate their C-terminal mature domain, which is approximately 15 KDa (4). The pro domain has been shown to play a role in proper protein folding (5) and protein precursor stabilization (6). Proteolytic cleavage is performed by members of the subtilisin-like proprotein convertase (SPC) family, which hydrolyze the peptide bond succeeding the R-X-X-R motif recognized by these proteases (7). Two examples of such proteases are Furin and Pace4, which have been shown to play a role in Nodal and BMP4 processing and signaling (8).

The TGF-β functional unit is a covalently linked dimer (Figure 1-1), which can exist as a homodimer and, in rare instances, as a heterodimer (9,10). Most TGF-β ligands have 7 cysteine residues in each monomer, which

allow them to form the so-called cysteine knot motif (11), one of the characteristic features of this class of proteins.

The cysteine knot is defined by the sequence C_1-X_n-C_2-X-G-X-C_3-X_n-C-C_4-X_n-C_5-X-C_6 where X_n represents the number of residues between cysteines, which can vary from ligand to ligand, and C represents a Cysteine residue. An 8-residue ring is formed by disulfide bonds established between C2/C5 and C3/C6, with a disulfide bond between C1 and C4 going through the middle of this ring (Figure 1-1, insert). The Glycine residue located in the middle of the sequence acts as an important stereochemical element, and the Cys residue N-terminally adjacent to C4 establishes the intermolecular disulfide bond responsible for joining the two monomers.

Each TGF-β monomer has 2 beta sheets, also referred to as the "fingers" of the ligand (fingers f1 and f2, Figure 1-1), that extend outward from an alpha helix, referred to as the "knuckle" of the ligand (H3, figure 1-1), giving it a butterfly shape (12). Hydrophobic interactions, along with the interdisulfide bond, stabilize the dimer (3).

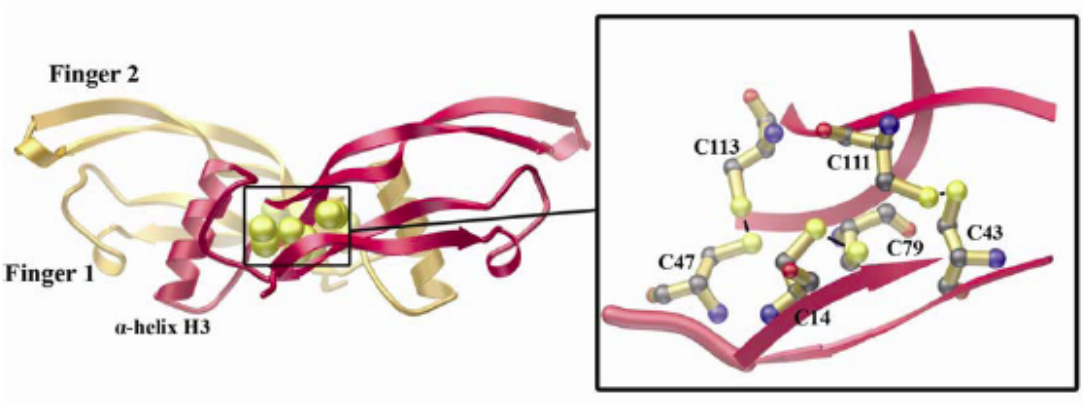

Figure 1-1: The TGF-β ligand, with a close up of the cysteine knot motif (from ref. 13; Allendorph). Monomers are shown in yellow and red. Cysteines are depicted as spheres.

TGF-β ligands play a role in a plethora of biological functions such as the development, maintenance, regeneration of tissues and organs (14,15), bone formation, maintenance of pluripotency in human embryonic stem cells (hESCs), growth and differentiation of various cell types (16), and vascular morphogenesis (17), to name a few. Intriguingly, these ligands use only two main signaling pathways to elicit all these biological responses.

TGF-β Signaling

TGF-β ligands utilize only 12 receptors for signal transduction: seven type I receptors (also known as signal propagating components) and five type II receptors (also known as activator components) (18,19). Both types of receptors are Serine/Threonine kinases. All of these receptors are approximately 500 amino acids in length, and share a common architecture: a N-terminal extracellular ligand binding domain exhibiting a characteristic 3-finger toxin fold comprised of 7 beta strands forming 3 antiparallel beta sheets

held together by 4 intradisulfide bonds (20), a transmembrane domain, and a C-terminal kinase domain (3). Type I receptors share structural features among each other that are not seen in type II receptors, such as the spacing of cysteine residues in its extracellular region and a conserved Glycine-Serine rich region, which plays a role in receptor phosphorylation and regulation of catalytic activity (21,22) (Figure 1-2).

Interestingly, ligand interactions with type II receptors do not seem to be as conserved as ligand interaction with type I receptors. Thus, several ligands that have high affinity for the same type II receptor may exhibit different binding interfaces (3). These observations suggest that type II receptors may play a more important role than type I receptors in determining specificity for the assembly of signaling complexes (3).

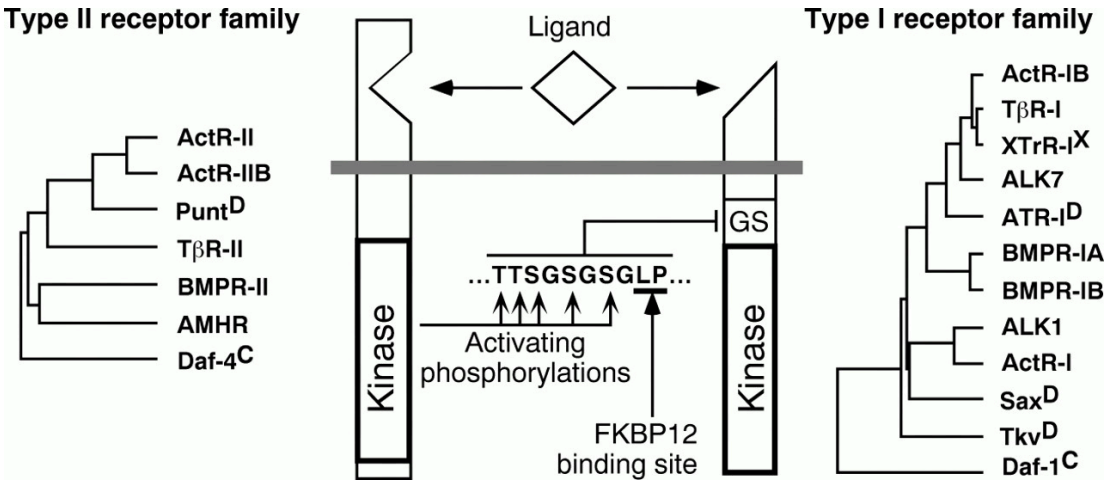

Figure 1-2: The type I and type II receptor families (from ref. 22; Massagué). Type I receptors have a GS rich region which acts as the site for receptor phosphorylation.

It can be inferred that an exquisite interplay of binding affinities occurs in order for proper gene regulation by these ligands. Thus, ligands exhibit binding selectivity for certain receptors. TGF-β binds preferentially to the TGFβR1 (also known as TβR1 or ALK5) type I receptor and the TGFβR2 type II receptor. Activin and Nodal share an affinity for type I receptors ACVR1 (ALK2, ActRI), ACVR1B (ALK4, ActRIB), and ACVR1C (ALK7) and for type II receptors ACVR2A (ActRII) and ACVR2B (ActRIIB). BMPs on the other hand have an affinity for type I receptors BMPRIA (ALK3) and BMPRIB (ALK6) and share an affinity for type II receptors ActRII and ActRIIB with Activin and Nodal, in addition to binding type II receptor BMPR2 (19).

In order to initiate a signaling cascade, TGF-β ligands form signaling complexes with their respective type I and II receptors. The signaling complex is composed of two type I receptors bound to the “wrist” epitopes of the dimerized ligand and two type II receptors bound to the “fingers” of the ligand, forming a hexameric complex (Figure 1-3). The order in which the signaling complex is assembled, as well as its receptor composition, varies between TGF-β subfamilies, as each subfamily exhibits particular affinities for type I and type II receptors and levels of ligand plasticity that dictate the order the ligand will bind to its receptors.

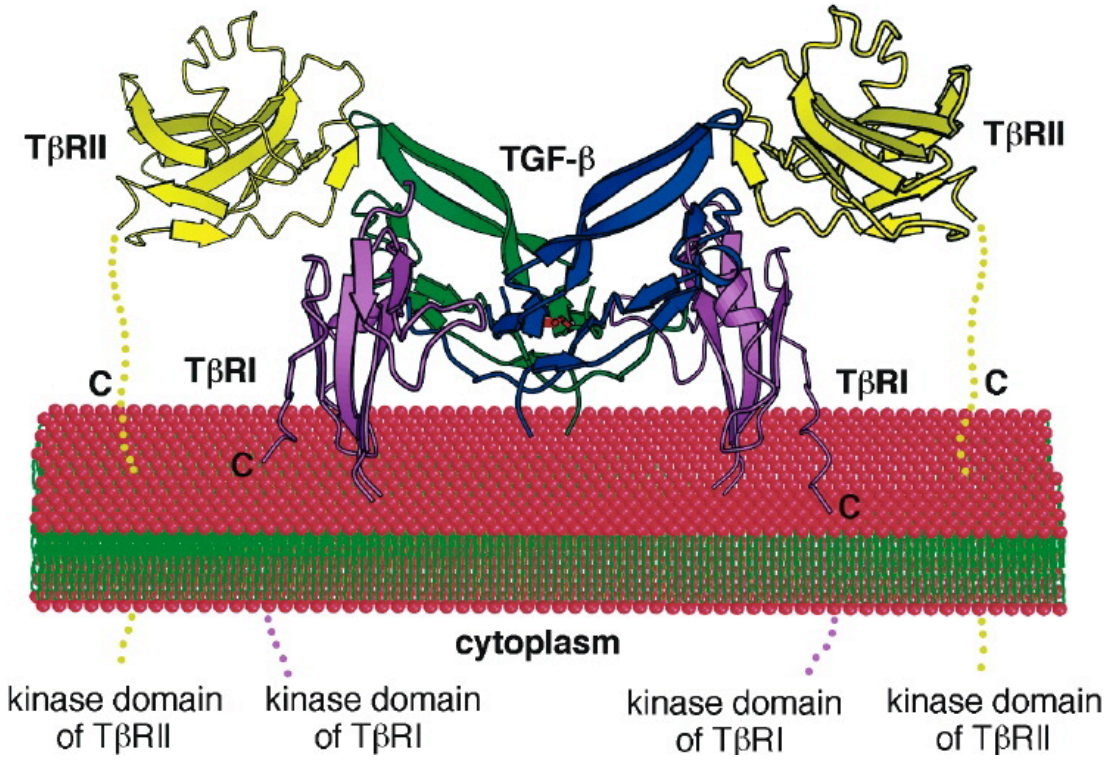

Figure 1-3: Assembled TGF-β signaling complex (from ref. 3; Shi, Massagué). Type I receptors are shown in purple, binding to the wrist epitope of the ligand. Type II receptors are shown in yellow, binding to the fingers of the ligand.

In the case of BMP signaling complex formation, BMPs have a higher affinity for the type I receptor, and thus will bind to it first. Structural studies have shown that BMP binds to its type I receptor on its “wrist” epitope using a knob-in-hole model, in which a hydrophobic residue from the receptor (usually a Phe) is positioned inside a hydrophobic pocket formed by the ligand. The residues involved in type I receptor binding are highly conserved across TGF-β ligands and receptors (23), and it is important to note that the pair of type I receptors establish contacts with both ligand monomers but do not contact each other (23). After binding to their type I receptors, the ligand-receptor complex binds to its type II receptors, which initiate the signaling cascade.

TGF-β and Activin ligands assemble their signaling complexes differently, binding to their type II receptors first. In the case of Activin, it is believed that binding of the type II receptors stabilizes this flexible ligand and allows it to recruit its type I receptors (24). The ligand-receptor complex is then recognized by the type I receptors, which in turn form the ternary complex required for signaling (21). TGF-β, as well as Nodal, require an accessory protein that acts as a co-receptor and allows the ligand to recruit and bind to its receptors. Two such proteins are β-glycan, which allows TGF-β to bind to its receptors (19), and Cripto, an EGF-CFC protein that plays a crucial role in Nodal binding to its receptors (25).

After complex formation, signaling is initiated by phosphorylation of the type I receptor by the constitutively active type II receptor. The type I receptor then phosphorylates receptor Smads (R-Smads), which are signal transducing molecules located near the cell membrane. The type of R-Smads that get phosphorylated by the ligand receptor complex depends on the ligand that binds to the receptor and will dictate the biological outcome of the signaling complex. In the case of TGF-β ligands Nodal and Activin, Smads 2 and 3 are phosphorylated, whereas in the case of BMP and GDFs Smads 1,5, and 8 are used for signal transduction (Figure 1-4). After phosphorylation, the R-Smads form a hetero- or homomeric complex with co-Smad Smad4, subsequently accumulating in the nucleus and ultimately regulating gene expression in conjunction with transcription factors (26) (Figure 1-5).

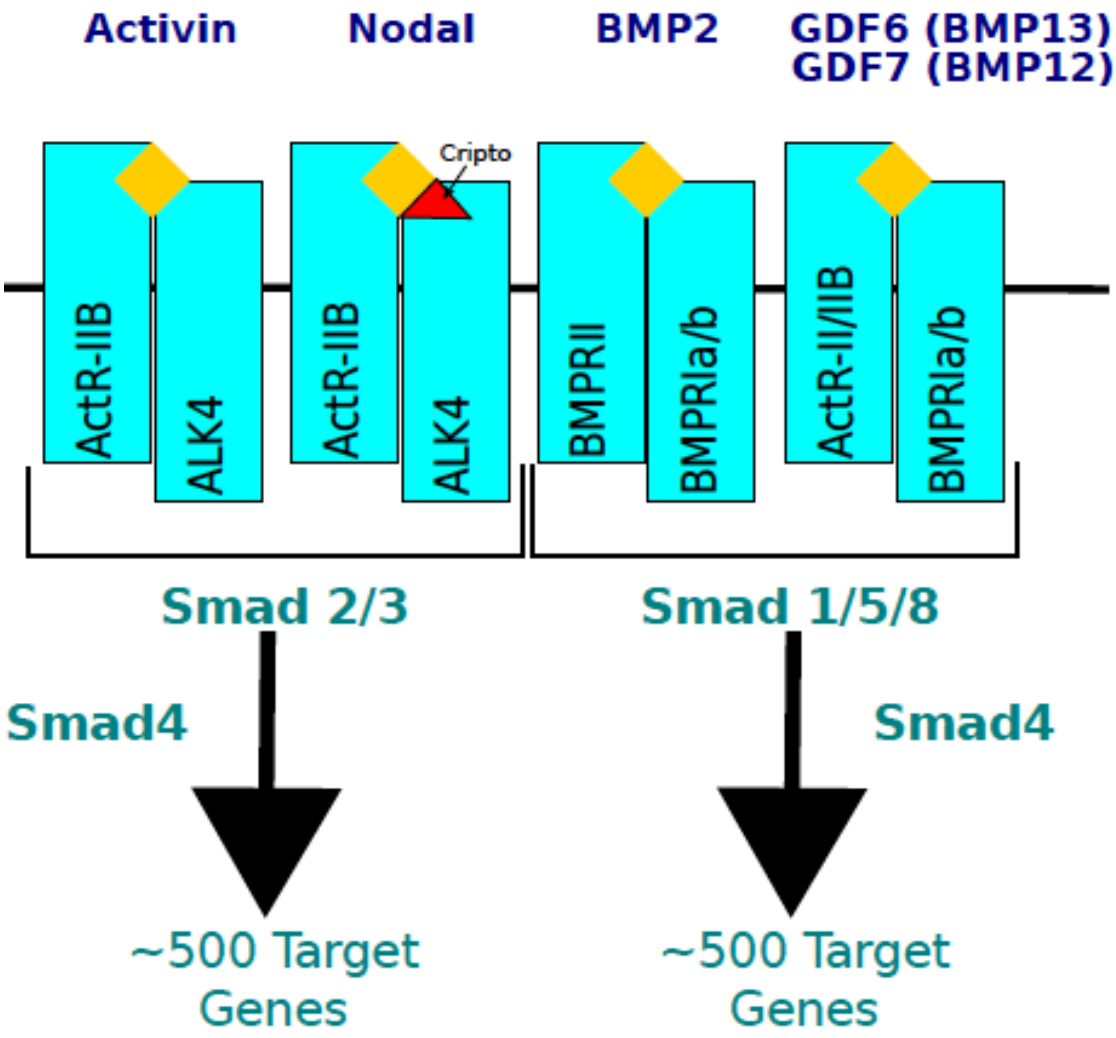

Figure 1-4: Receptor complexes and signaling pathways for Activin, Nodal, BMP2, and GDF6/7 ligands. Ligands are depicted in yellow, receptors are depicted in blue, and co-receptor Cripto is depicted in red.

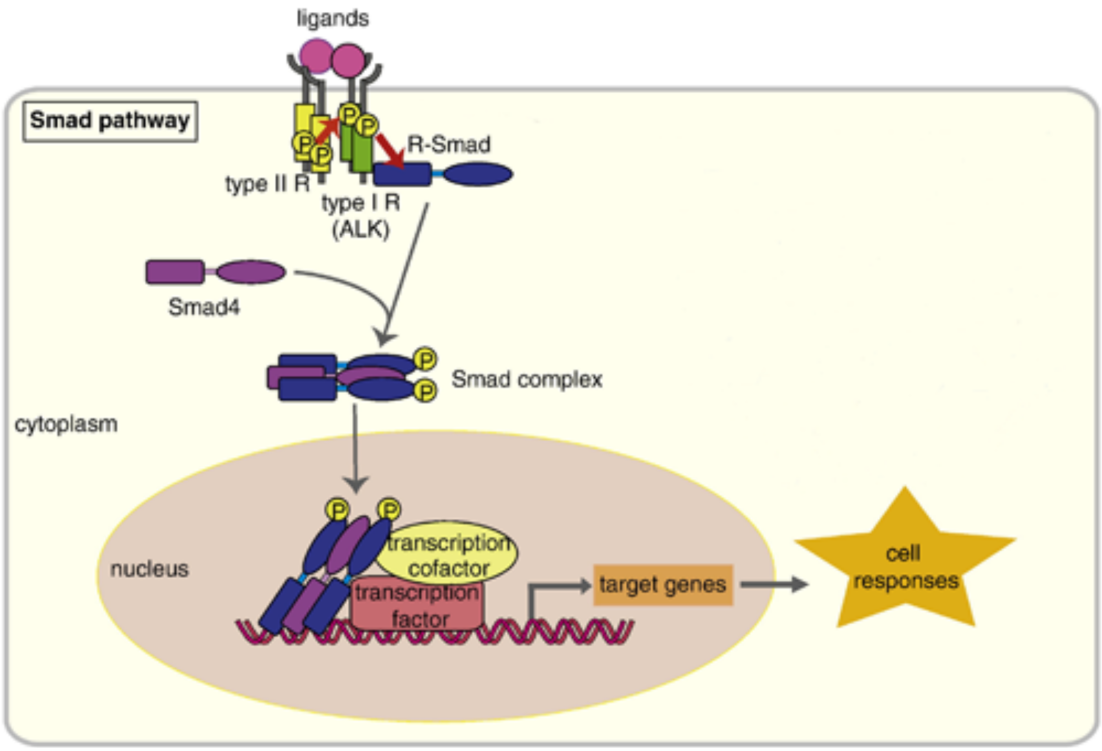

Figure 1-5: Schematic representation of the Smad signaling cascade (adapted from ref. 2; Sakaki-Yumoto, Katsuno, Derynck).

TGF-β signaling in the cell is tightly regulated using a combination of determinants such as the availability of unbound ligand capable of binding to the receptors, spatio-temporal expression of ligands and receptors, and binding affinity. Ligand access to receptors is regulated by a group of proteins collectively known as ligand traps, which block the ligand surfaces required for receptor binding (3). Two such ligand traps are Noggin, which is known to block BMP signaling (27) and Lefty, which blocks Nodal signaling (28). Both of these proteins prevent signaling complex formation by binding to their respective ligands, thus blocking their receptor binding epitopes.

Binding affinities between TGF-β ligands and their receptors are dictated at the amino acid level, with a single amino acid substitution having

the potential to radically change receptor affinities. One study has shown that one amino acid substitution in BMP2 can create a variant that has high affinity for ActRIIB (29), while another study has shown that a single residue in GDF5 is responsible for binding specificity to BMPRIB (14). Given these findings, it can be seen that residues that directly impact the surface properties and binding affinities to receptors are responsible for ligand/receptor assembly and have a significant effect on the intensity and temporal aspects of signaling. Therefore, structural studies of TGF-β ligands and their receptors play a key role in understanding the intricacies and nuances of TGF-β signaling complex formation. Of particular note are Activin, Nodal, and GDF6 and 7, four ligands that, despite being members of different TGF-β subfamilies, share the same type II receptor with similar affinity.

Activin, GDF6, GDF7, and Nodal

Activin, GDF6 (also known as BMP13), GDF7 (also known as BMP12) and Nodal are four members of the TGF-β superfamily that pertain to two different sub families. All four are growth factors that induce the growth and differentiation of various cell types.

Activin plays a role in a wide range of biological processes ranging from erythropoiesis (30), Follicle Stimulating Hormone secretion (31), and differentiation of macrophages (32) to the establishment of joints, skeleton, and cartilage formation (33,34,35). GDF6 and GDF7 have been associated with tendon and ligament formation and repair (16), with GDF6 being highly conserved among a wide range of vertebrate species (33).

Nodal plays an important role in early embryonic development, (37,38) particularly in left-right axis asymmetry and mesoderm formation (39). It has also been observed to play a role in maintaining pluripotency of human embryonic stem cells (hESCs) (40) and in the propagation of mouse ESCs (41). Additionally, it has been found that even though Nodal supports cardiomyocite development in BMP induced cells, prolonged Nodal signaling inhibits cardiac specification (42).

Remarkably, these ligands share signaling receptors despite having very different roles. Both Activin and Nodal transmit their signals via the Activin type II (ActRII/IIB) and type I (ALK4) serine/threonine kinase receptors, and both GDF6 and GDF7 share an affinity for the type II receptor ActRII/IIB with Activin and Nodal.

Nodal signaling requires Cripto, a co-receptor from the Epidermal Growth Factor-Cripto/FRL1/Cryptic protein family. Although not required for signaling, Cripto can also bind and regulate Activin signaling by forming a complex with reduced signaling capacity (Figure 1-6) (43).

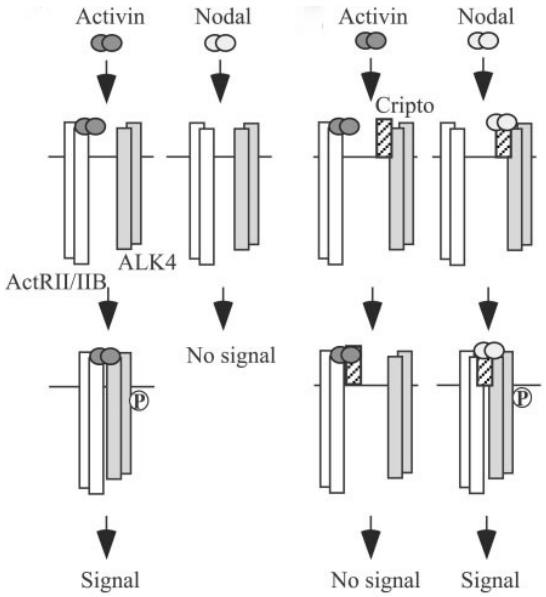

Figure 1-6: Schematic of Activin and Nodal signaling (from ref. 43; Gray, Harrison, Vale). Notice that Cripto is required for Nodal signaling and blocks signal transduction when bound to Activin.

Two important components of the Nodal and Activin signaling pathways are ALK4 and Cripto. ALK4 (also known as ActRIB) is a type I transmembrane serine/threonine receptor kinase that plays a pivotal role in Activin signal transduction (44). It has been shown that ALK4 plays a role in the regulation of left-right axis determination and mesoderm induction in *Xenopus* (45) and zebrafish (46), as well as in neuronal differentiation (47). Like all type I receptors, ALK4 shows ligand binding activity in its extracellular domains and kinase activity in its intracellular domains (48).

Cripto is a GPI anchored co-receptor that plays a significant role in the activation of the Nodal/ALK4/ALK7/Smad-2 signaling pathway (49). Studies have suggested that Cripto may interfere with Activin's role in tumor

suppression by binding to ALK4 (49). Cripto binds to ALK4 through its CFC domain (50).

The GDF6 and GDF7 signaling receptor complexes are comprised of both type I and type II receptors bound as heterotetrameric complexes (16). Both ligands exhibit high affinity for the ALK6 (BMPRIB) and ALK3 (BMPRIA) type I receptors, which have been associated with chondrogenesis and vascular diseases (51,52). Furthermore, these ligands have an affinity for type II receptor ActRIIB comparable to the one exhibited for their type I receptor (16).

ActRII's affinity for Nodal, Activin, and GDFs is intriguing, given that these ligands exhibit markedly different levels of flexibility, with Activin being the most flexible (Figure 1-7). Thus, the elucidation of the structure of these ligands will provide valuable insight into how their flexibility plays a role in their functional properties. Furthermore, these structures will be a crucial first step in determining the mechanics involved in signaling complex formation.

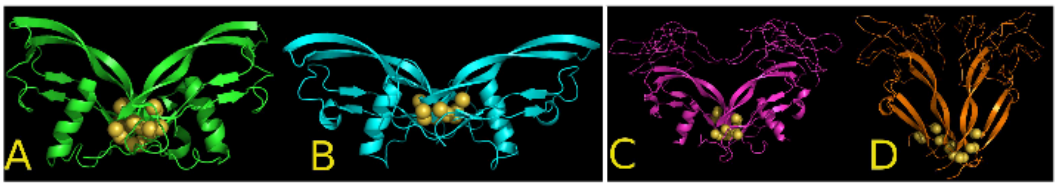

Figure 1-7: Structure comparison between A) Free Activin A, B) BMP2, C) Activin A/ActRIIB-ECD complex from Greenwald et al. (24) D) Activin A/ActRIIB-ECD complex from Thompson, Woodruff, Jardetzky (53).

Interestingly, all of these ligands play a role in musculoskeletal development despite using two different signaling pathways. Activin and Nodal signal through the Smad 2/3 pathway, whereas GDF6 and GDF7 signal

through the Smad 1/5/8 pathway used by BMPs. Therefore, I decided to focus on the role Activin/Nodal and BMP signaling play in this biological process by studying the structural features that allow these ligands to signal through these pathways. In order to elucidate these features, chimeric ligands were created by combining and assessing which ligand segments were relevant for signaling.

The study of the Activin/Nodal signaling pathway has been hindered by the difficulty to produce these ligands in the quantities required for extensive analysis. Indeed, the unavailability of Nodal has significantly hindered studies of this protein (54,55). Efforts at producing these ligands using a widely used chemical refolding protocol (56) which has proven effective for producing GDF6 and GDF7 failed for both Nodal and Activin. Thus, a novel strategy was used, developed by the Choe lab at the Salk Institute and termed Random Assembly of Segmental Chimera and Heteromers (RASCH). The RASCH strategy takes advantage of BMP2's high refolding efficiency to produce not only properly refolded chimeras with the properties of their parental ligands, but also chimeras that exhibit novel signaling characteristics.

The RASCH strategy involves dividing two parental proteins (either Activin or Nodal and BMP2) into 6 sections (conserving structural motifs) and recombining them using overlapping PCR techniques (Figure 1-8) (57). The chimeric constructs are then expressed in *Escherichia coli* inclusion bodies, denatured, and refolded. Finally, a two-step purification protocol using affinity and reverse phase chromatography is applied in order to obtain properly

refolded chimeric ligands that can be used for functional and structural studies. By combining Activin or Nodal sequences with BMP2 sequence members of the Choe Lab created AB2 and NB2 libraries, respectively. Two classes of chimeras were produced: 1) chimeras that mimic parental proteins and 2) chimeras that exhibit novel properties and/or enhanced parental properties. These chimeras are defined by the code (XXXXXX), where X=N/A (Nodal/Activin) or B (BMP2), depending on which segment is in position X.

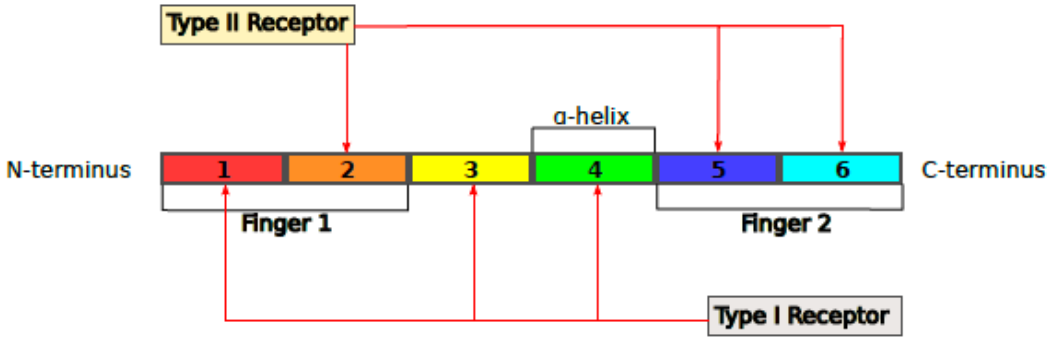


```
                                1                                2                                3
BMP2          1  QAKHKQRKRLKSSCKRHPLYVDFSDVGWNDWIVAPPGYHAFYCHGECPFPLADHLNSTNH 60
Activin-βA    1  --GLECDGKVNICCKKQ-FFVSFKDIGWNDWIIAPSGYHANYCEGECPSHIAGTSGSS-L 56

BMP2         61  AIVQTLVN----SVNSKIP--KACCVPTELSAISMLYLDENEKVVLKNYQDMVVEGCGCR 114
Activin-βA   57  SPHSTVINHYRMRGHSPFANLKSCCVPTKLRPMSMLYYDDGQNIIKKDIQNMIVEECGCS 116
                                    4                5                6

                                1                                2                                3
BMP2          1  QAKHKQRKRLKSSCKRHPLYVDFSDVGWNDWIVAPPGYHAFYCHGECPFPLADHLNSTNH 60
Nodal         1  ---HHLPDRSQ-LCRKVKFQVDFNLIGWGSWIIYPKQYNAYRCEGECPNPVGEEFHPTNH 56

BMP2         61  AIVQTLVNSVN-SKIPKACCVPTELSAISMLYLDENEKVVLKNYQDMVVEGCGCR 114
Nodal        57  AYIQSLLKRYQPHRVPSTCCVPVKTKPLSMLYVD-NGRVVLDHHKDMIVEECGCL 110
                                    4                5                6
```

Figure 1-8: Segment swapping strategy using the RASCH methodology. The top diagram indicates the structural feature each segment forms in the ligand.

At least one NB2 chimera, NB250, has been shown to be functionally identical to Nodal and can be produced in the amounts required for structural studies. Furthermore, previous studies have demonstrated that chimera AB208 from the AB2 library exhibits the signaling properties of Activin (57). Additionally, the RASCH strategy yielded other chimeras, such as AB204, with enhanced Smad 1/5/8 signaling capabilities compared to wild type BMP2, and both AB2 and NB2 chimeras have demonstrated enhanced osteogenic and chondrogenic properties, respectively, which are equivalent or surpass those observed for BMP2, the parental ligand shared by both chimera libraries.

Here, I present the structures of 2 chimeric ligands that mimic Nodal (NB250) and Activin (AB208), in addition to the structures of two members of the GDF subset of BMP proteins (GDF6, GDF7). Furthermore, the structure of an AB2 chimera with enhanced osteogenic properties (AB204) is presented. Using the structures elucidated, mechanistic models are proposed to account for the chimeric ligands' enhanced signaling and functional properties, as well as for the functional properties of GDF6 and GDF7.

The elucidation of the structures of these ligands and their complexes will be used to guide mutagenesis of ligands and chimeras in order to understand the structure/function relation in osteo-, teno-, and chondrogenesis. Furthermore, these discoveries could also be applied for the design of therapeutic agents.

References

1. Huminiecki L, Goldovsky L, Freilich S, Moustakas A, Ouzounis C, Heldin C (2009) Emergence, development and diversification of the TGF-β signalling pathway within the animal kingdom. *BMC Evolutionary Biology* **9**: 28.

2. Sakaki-Yumoto M, Katsuno Y, Derynck R (2013) TGF-β family signaling in stem cells. *Biochimica et Biophysica Acta* **1830**: 2280-2296.

3. Shi Y, Massagué J (2003) Mechanisms of TGF-beta signaling from cell membrane to the nucleus. *Cell* **113**: 685-700.

4. Cui Y, Hackenmiller R, Berg L, Jean F, Nakayama T, Thomas G, Christian JL (2001) The activity and signaling range of mature BMP-4 is regulated by sequential cleavage at two sites within the prodomain of the precursor. *Genes Dev* **15**: 2797-2802.

5. Sopory S, Nelsen S, Degnin C, Wong C, Christian J (2006) Regulation of bone morphogenetic protein-4 activity by sequence elements within the prodomain. *J Biol Chem* **281**: 34021-34031.

6. Le Good J, Joubin K, Giraldez A, Ben-Haim N, Beck S, Chen Y, Schier AF, Constam DB (2005) Nodal stability determines signaling range. *Current biology* **15**:31-36.

7. Constam D, Robertson E (1999) Regulation of bone morphogenetic protein activity by pro domains and proprotein convertases. *The Journal of cell biology* **144**:139-149.

8. Beck S, Le Good J, Guzman M, Ben Haim N, Roy K, Beermann F, Constam DB (2002) Extraembryonic proteases regulate Nodal signalling during gastrulation. *Nature cell biology* **4**: 981-985.

9. Lin S, Lerch T, Cook R, Jardetzky T, Woodruff T (2006) The structural basis of TGF-beta, bone morphogenetic protein, and activin ligand binding. *Reproduction* **132**:179-190.

10. Chang C, Hemmati-Brivanlou A (1999) Xenopus GDF6, a new antagonist of noggin and a partner of BMPs. *Development* **126**: 3347–3357.

11. McDonald NQ, Hendrickson WA (1993) A Structural Superfamily of Growth Factors Containing a Cysteine Knot Motif. *Cell* **73**: 421-424.

12. Daopin S, Piez KA, Ogawa Y, Davies DR (1992) Crystal structure of transforming growth factor-β2: An unusual fold for the superfamily. *Science* **257**: 369-373.

13. Allendorph GP (2007) *X-ray Crystallographic and Biochemical Studies on the Bone Morphogenetic Protein Family* (Doctoral dissertation). Retrieved from ProQuest Dissertations and Theses. Accession order No. 327812.

14. Nickel J, Kotzsch A, Sebald, W, Mueller T (2005). A single residue of GDF-5 defines binding specificity to BMP receptor IB. *Journal of molecular biology* **349**: 933-947.

15. den Hollander AI, Biyanwila J, Kovach P, Bardakijan T, Traboulsi EI, Ragge NK, Schneider A, Malicki J (2010) Genetic defects of GDF6 in the zebrafish out of sight mutant and in human eye developmental anomalies. *BMC Genetics* **11**: 102.

16. Berasi SP, Varadarajan U, Archambault J, Cain M, Souza TA, Abouzeid A, Li J, Brown CT, Dorner AJ, Seeherman HJ, Jelinsky SA (2011) Divergent activities of osteogenic BMP2, and tenogenic BMP12 and BMP13 independent of receptor binding affinities. *Growth Factors* **29**: 128-139.

17. Pardali E, Goumans M, ten Dijke P (2010) Signaling by members of the TGF-beta family in vascular morphogenesis and disease. *Trends Cell Biol* **20**: 556-567.

18. Nickel J, Sebald W, Groppe JC, Mueller TD (2009) Intricacies of BMP receptor assembly. *Cytokine & Growth Factor Reviews* **20**: 367-377.

19. Massagué J (2012) TGFβ signalling in context. *Nat Rev Mol Cell Biol* **13**: 616-630.

20. Greenwald J, Fischer W, Vale W, Choe S (1999) Three-finger toxin fold for the extracellular ligand-binding domain of the type II activin receptor serine kinase. *Nat Struct Biol* **6**: 18-22.

21. Wrana J, Attisano L, Wieser R, Ventura F, Massagué J (1994) Mechanism of activation of the TGF-β receptor. *Nature* **370**: 341-347.

22. Massagué J (1997) TGF-beta signal transduction. *Annual review of biochemistry* **67**: 753-791.

23. Kirsch T, Sebald W, Dreyer M (2000) Crystal structure of the BMP-2-BMPRIA ectodomain complex. *Nat Struct Biol* **7**: 492-496.

24. Greenwald J, Vega M, Allendorph G, Fischer W, Vale W, Choe S (2004) A Flexible Activin Explains the membrane-Dependent Cooperative Assembly of TGF-beta Family Receptors. *Molecular Cell* **15**: 485-489.

25. Gritsman K, Zhang J, Cheng S, Heckscher E, Talbot W, Schier A (1999) The EGF-CFC Protein One-Eyed Pinhead Is Essential for Nodal Signaling. *Cell* **97**: 121-132.

26. Ross S, Hill C (2008) How the Smads Regulate Transcription. *The International Journal of Biochemistry & Cell Biology* **40**: 383-408.

27. Groppe J, Greenwald J, Wiater E, Rodriguez-Leon J, Economides A, Kwiatkowski W, Affolter M, Vale WW, Izpisua Belmonte JC, Choe S (2002) Structural basis of BMP signalling inhibition by the cystine knot protein Noggin. *Nature* **420**: 636-642.

28. Schier A (2009) Nodal Morphogens. *Cold Spring Harbor perspectives in biology* **1**: a003459.

29. Weber D, Kotzsch A, Nickel J, Harth S, Seher A, Mueller U, Sebald W, Mueller TD (2007). A silent H-bond can be mutationally activated for high-affinity interaction of BMP-2 and activin type IIB receptor. *BMC Struct Biol* **7**: 6.

30. Shiozaki M, Sakai R, Tabuchi M, Nakamura T, Sugino K, Sugino H, Eto Y (1992) Evidence for the participation of endogenous activin A/erythroid differentiation factor in the regulation of erythropoesis. *Proc. Natl. Acad. Sci. USA* **89**: 1553-1556.

31. Rivier C, Vale W (1991) Effect of Recombinant Activin-A on Gonadotropin Secretion in the Female Rat. *Endocrinology* **129**: 2463-2465.

32. Ogawa K, Funaba M, Chen Y, Tsujimoto M (2006) Activin-A functions as a Th2 cytokine in the promotion of the alternative activation of macrophages. *J Immunol* **177**: 6787-6794.

33. Williams LA, Bhargav D, Diwan AD (2008) Unveiling the Bmp13 Enigma: Redundant Morphogen or Crucial Regulator? *International Journal of Biological Sciences* **4**: 318-329.

34. Merino R, Macias D, Gañan Y, Rodriguez-Leon J, Economides AN, Rodriguez-Esteban C, Izpisua-Belmonte JC, Hurle JM (1999) Control of digit formation by Activin signaling. *Development* **126**: 2161-2170.

35. Montero J, Lorda-Diez C, Gañan Y, Macias D, Hurle J (2008) Activin/TGFbeta and BMP crosstalk determines digit chondrogenesis. *Developmental biology* **321**: 343-356.

36. Furue M, Myoishi Y, Fukui Y, Ariizumi T, Okamoto T, Asashima M (2002) Activin A induces craniofacial cartilage from undifferentiated Xenopus ectoderm in vitro. *Proc. Natl. Acad. Sci. USA* **99**: 15474-15479.

37. Zhou X, Sasaki H, Lowe L, Hogan BL, Kuehn MR (1993) Nodal is a novel TGF-β-like gene expressed in the mouse node during gastrulation. *Nature* **361**: 543-547.

38. Conlon FL, Lyons KM, Takausu N, Barth KS, Kispert A, Herrmann B, Robertson EJ (1994) A primary requirement for nodal in the formation and maintenance of the primitive streak in the mouse. *Development* **120**: 1919-1928.

39. Tsuchida K, Nakatani M, Uezumi A, Murakami T, Cui X (2008) Signal transduction pathway through activin receptors as a therapeutic target of musculoskeletal diseases and cancer. *Endocr J* **55**: 11-21.

40. Vallier L, Mendjan S, Brown S, Chng Z, Teo A, Smithers LE, Trotter MW, Cho CH, Martinez A, Rugg-Gunn P, Brons G, Pedersen RA (2009) Activin/Nodal signaling maintains pluripotency by controlling Nanog expression. *Development* **136**: 1339-1349.

41. Ogawa K, Saito A, Matsui H, Suzuki H, Ohtsuka S, Shimosato D, Morishita Y, Watabe T, Niwa H, Myazono K (2007) Activin-Nodal signaling is involved in propagation of mouse embryonic stem cells. *J Cell Sci* **120**: 55-65.

42. Kattman SJ, Witty AD, Gagliardi M, Dubois NC, Niapour M, Hotta A, Ellis J, Keller G (2011) Stage-specific optimization of activin/nodal and BMP signaling promotes cardiac differentiation of mouse and human pluripotent stem cell lines. *Cell Stem Cell* **8**: 228-240.

43. Gray P.C., Harrison C.A., Vale W (2003) Cripto forms a complex with Activin and type II Activin receptors and can block Activin signaling. *Proc. Natl. Acad. Sci. USA* **100**: 5193-5198.

44. Harrison CA, Gray PC, Koerber SC, Fischer W, Vale W (2003) Identification of a Functional Binding Site for Activin on the Type I Receptor ALK4. *J Biol Chem* **278**: 21129-21135.

45. Chen D, Zhao M, Mundy GR (2004) Bone morphogenetic proteins. *Growth Factors* **4**: 233-241.

46. Sun Z, Jin P, Tian T, Gu Y, Chen Y, Meng A (2006) Activation and roles of ALK4/ALK7-mediated maternal TGFβ signals in zebrafish embryo. *Biochemical and Biophysical Research Communications* **345**: 694-703.

47. Suzuki K, Kobayashi T, Funatsu O, Morita A, Ikekita M (2010) Activin A induces neuronal differentiation and survival via ALK4 in a SMAD-independent manner in a subpopulation of human neuroblastomas. *Biochemical and Biophysical Research Communications* **394**: 639-645.

48. Harrison C.A., Wiater E, Gray P.C., Greenwald J, Choe S, Vale W (2004) Modulation of Activin and BMP signaling. *Molecular and Cellular Endocrinology* **225**: 19-24.

49. Strizzi L, Bianco C, Normanno N, Salomon D (2005) Cripto-1: a multifunctional modulator during embryogenesis and oncogenesis. *Oncogene* **24**: 5731-5741.

50. Calvanese L, Saporito A, Oliva R, D'Auria G, Pedone C, Paolillo L, Menotti R, Marasco D, Falcigno L (2008) Structural insights into the interaction between the Cripto CFC domain and the ALK4 receptor. *Journal of Peptide Science* **15**: 175-183.

51. Cai J, Pardali E, Sánchez-Duffhues G, ten Dijke P (2012) BMP signaling in vascular diseases. *FEBS letters* **586**: 1993-2002.

52. Yi SE, Daluiski A, Pederson R, Rosen V, Lyons KM (2000) The type I BMPR receptor BMPRIB is required for chondrogenesis in the mouse limb. *Development* **127**: 621-630.

53. Thompson T, Woodruff T, Jardetzky T (2003) Structures of an ActRIIB:Activin A complex reveal a novel binding mode for TGF-beta ligand:receptor interactions. *EMBO J.* **22**: 1555-1566.

54. Lonardo E, Hermann PC, Mueller MT, Huber S, Balic A, Miranda-Lorenzo I, Zagorac S, Alcala S, Rodriguez-Arabaolaza I, Ramirez JC, Torres-Ruiz R, Garcia E, Hidalgo M, Cebrian DA, Heuchel R, Lohr M, Berger F, Bartenstein P, Aicher A, Heeschen C (2011) Nodal/Activin signaling drives self-renewal and tumorigenicity of pancreatic cancer

stem cells and provides a target for combined drug therapy. *Cell Stem Cell* **9**: 433-446.

55. Pera MF, Tam PP (2010) Extrinsic regulation of pluripotent stem cells. *Nature* **465**: 713-720.

56. Groppe J, Rumpel K, Economides A, Stahl N, Sebald W, Affolter M (1998) Biochemical and Biophysical Characterization of Refolded Drosophila DPP, a Homolog of Bone Morphogenetic Proteins 2 and 4. *J Biol Chem* **273**: 29052-29065.

57. Allendorph G, Read J, Kawakami Y, Kelbe J, Isaacs M, Choe S (2011) Designer TGFb Superfamily Ligands with Diversified Functionality. *PLoS ONE* **6**:e26402.

Chapter 2. Designer Nodal/BMP2 chimeras mimic Nodal signaling, promote chondrogenesis, and reveal a BMP-2 like structure

Introduction

Nodal plays an important role in early embryonic development (1,2), particularly in mesoderm formation (3) and in establishing left-right (LR) asymmetry in vertebrates (4). The biochemical and biophysical studies of Nodal signaling have been hampered due to the inability to produce this protein in quantities suitable for structural and functional studies. The RASCH strategy has not only facilitated the production of properly refolded chimeras with the properties of their parental ligands, but also the production of chimeras that exhibit novel signaling characteristics.

In the case of Nodal, the RASCH strategy was used to combine Nodal and BMP2 to create Nodal/BMP2 chimeras (NB2 library). Three chimeras (NB250, NB260, and NB264) were identified with the refolding capabilities of BMP2 and the Cripto-dependent signaling properties of Nodal, and one (NB250) was identified as being able to mimic Nodal *in vivo*. Furthermore, it was discovered that in addition to NB250 and NB260 having Nodal-like properties, they are superior to BMP2 in promoting chondrogenic differentiation of human adipose-derived stem cells (hASC). These findings, coupled with previous studies that show that the Activin signaling pathway plays a role in chondrogenesis (5), suggest a new role for Nodal in chondrogenesis and demonstrate that NB250 can be used as a substitute for Nodal in structural/functional studies and as a possible therapeutic agent to treat cartilage damage.

Additionally, the crystal structure of NB250 was solved, demonstrating that its fundamental scaffold remains identical to that of BMP2 except for small local conformational changes in the receptor-binding regions. This novel structure suggests that the structure of Nodal may be more akin to BMPs than previously thought.

NB2 Chimeras are similar to Nodal in functional tests

Nodal is known to signal through the Smad 2/3 pathway (6). Therefore, in order to determine whether NB2 chimeras are able to signal in the same manner as Nodal, and in collaboration with the Vale Lab (Salk Institute), the Smad2 dependent luciferase induction potential of Nodal chimeras was tested by using a whole cell luciferase reporter assay sensitive to Smad2 activation. Results indicated that out of several screened chimeras three of them, namely NB250 (chimeric sequence BNNNBB), NB260 (BNNNBN), and NB264 (BNNNNN), stood out for Cripto-Smad2-dependent luciferase induction (Figure 2-1A).

Additionally, Cripto-dependent activation of phospho-Smad2 was tested by Western blotting. Results show that NB250, NB260, and NB264 activate phospho-Smad2 in a Cripto-dependent manner comparable to that of commercial Nodal (Figure 2-1B). These findings indicate that these chimeric ligands are signaling in a similar manner to Nodal, and that they require co-receptor Cripto to do so.

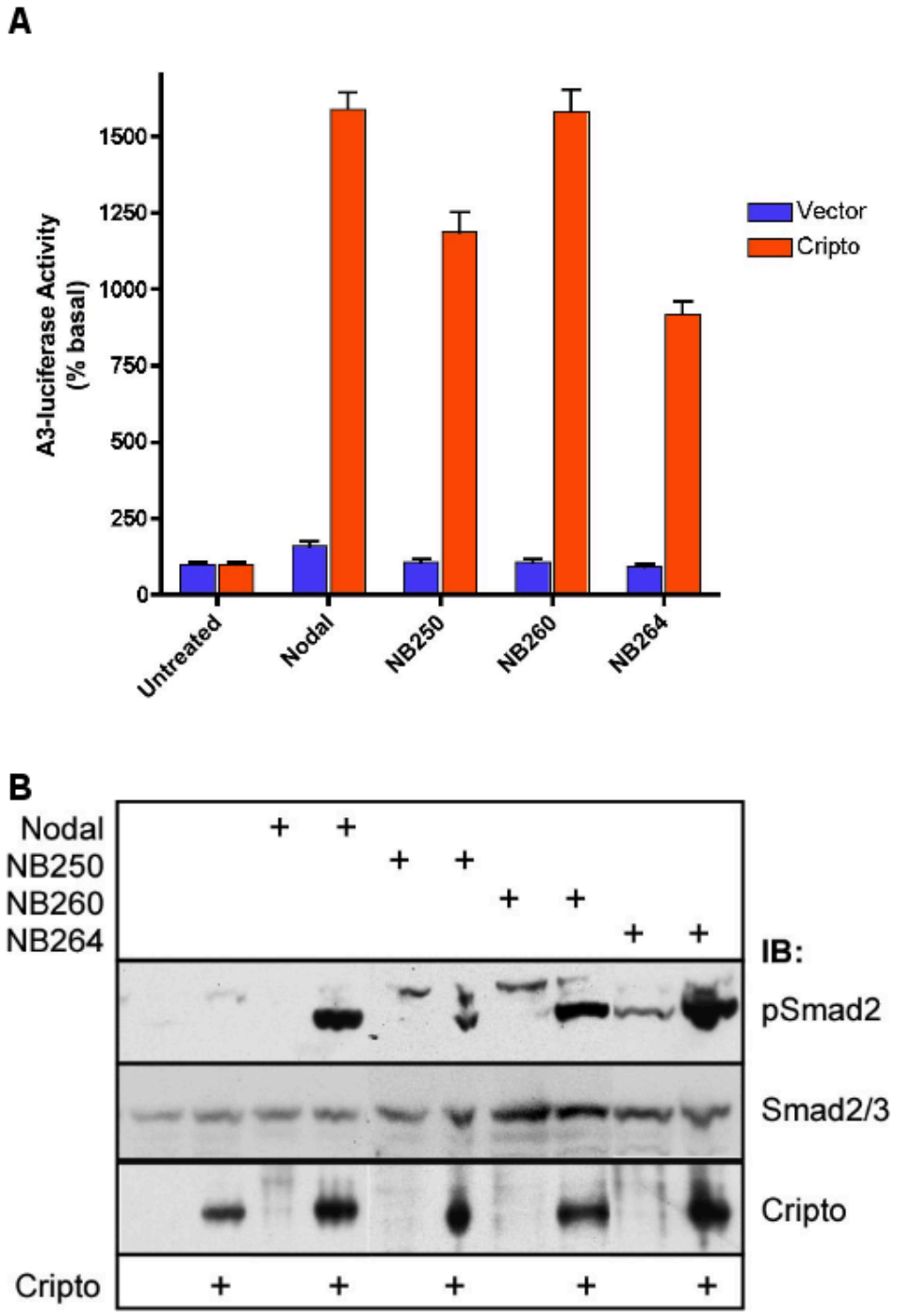

Figure 2-1: A) Smad2 responsive luciferase reporter assay. NB250, NB260, and NB264 show induction levels similar to commercially available Nodal. B) Cripto-dependent activation of phospho-Smad2 assay.

Given that NB250 holds the least sequence similarity to Nodal, yet it appears to signal and activate phospho-Smad2 in the same manner as Nodal, we sought to determine whether phospho-Smad2 activation is similarly dosage-dependent in NB250 as it is in Nodal (Figure 2-2). In the tested concentration range of 0.01 to 30nM activation of phospho-Smad2 by NB250 closely follows that of Nodal.

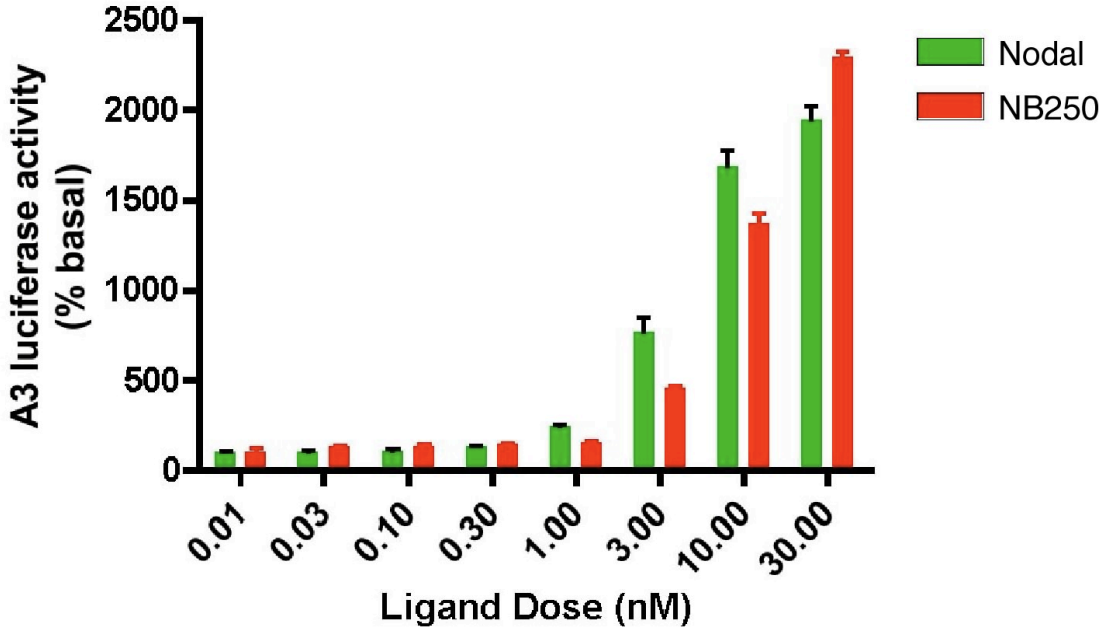

Figure 2-2: Commercial Nodal and NB250 exhibit similar Cripto-dependent activation of Smad2 signaling. 293T cells were treated with varying concentrations of commercially available Nodal and NB250, and their luciferase activity was measured.

Additionally, we decided to test whether this chimera was able to signal through the BMP2 signaling pathway. Using luciferase reporter assays, we determined that NB250 exclusively activates the Activin signaling pathway at the same levels as Nodal (Figure 2-3).

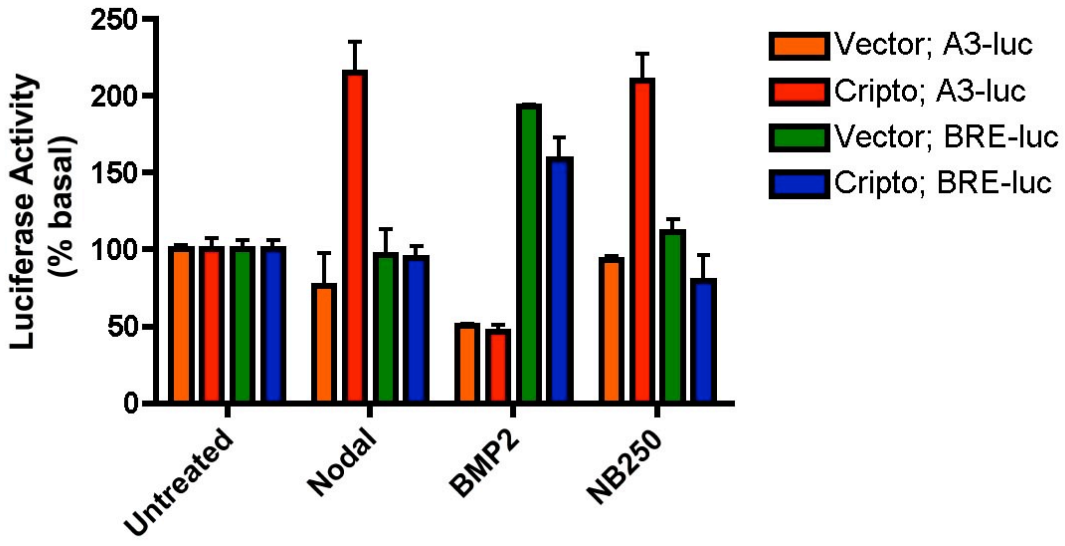

Figure 2-3: NB250 signaling resembles Nodal but not BMP2. Nodal, NB250 and BMP2 luciferase assay results using Activin response element (A3-luc) luciferase (to test for Smad2 signaling pathway activation) vs. BMP response element (BRE-luc) luciferase (to test for Smad 1/5/8 signaling pathway activation).

These results support our findings that NB250 is Cripto dependent and utilizes the same signaling pathway as Nodal. Furthermore, they also show that this chimeric ligand has a similar dosage effect on Smad2 signaling as Nodal.

NB250 mimics Nodal *in vivo*

One of the roles Nodal has in development is the induction of heart looping during the establishment of vertebrate embryonic left-right asymmetry by controlling the expression of the *Pitx2* gene, which is a transcription target that mediates left-right asymmetry in vertebrates (7). In order to determine whether NB250 mimics Nodal *in vivo*, and in collaboration with the Belmonte

Lab (Salk Institute), NB250's potential to regulate *Pitx2* expression and heart looping was tested using chick embryos.

During development, *Pitx2* transcripts are only detected on the left side of the lateral plate mesoderm in chick embryos (Figure 2-4A). However, both Nodal and NB250 are able to induce ectopic expression of *Pitx2* and alter heart looping during the establishment of vertebrate embryonic left-right asymmetry. Ectopic expression of Nodal on the right side of chick embryos leads to induction of *Pitx2* transcripts on this side of the lateral plate mesoderm (Figure 2-4B). Furthermore, the application of an NB250-soaked bead to the right side of the lateral plate mesoderm induces ectopic expression of *Pitx2* transcripts on the right lateral plate mesoderm (Figure 2-4C).

Even though the wild-type chick embryo develops with a rightward heart looping (Figure 2-4D), Nodal and NB250 were able to reverse heart looping to a leftward orientation in one third of the embryos tested (Figure 2-4E and F). These findings indicate that NB250 is able to functionally mimic Nodal.

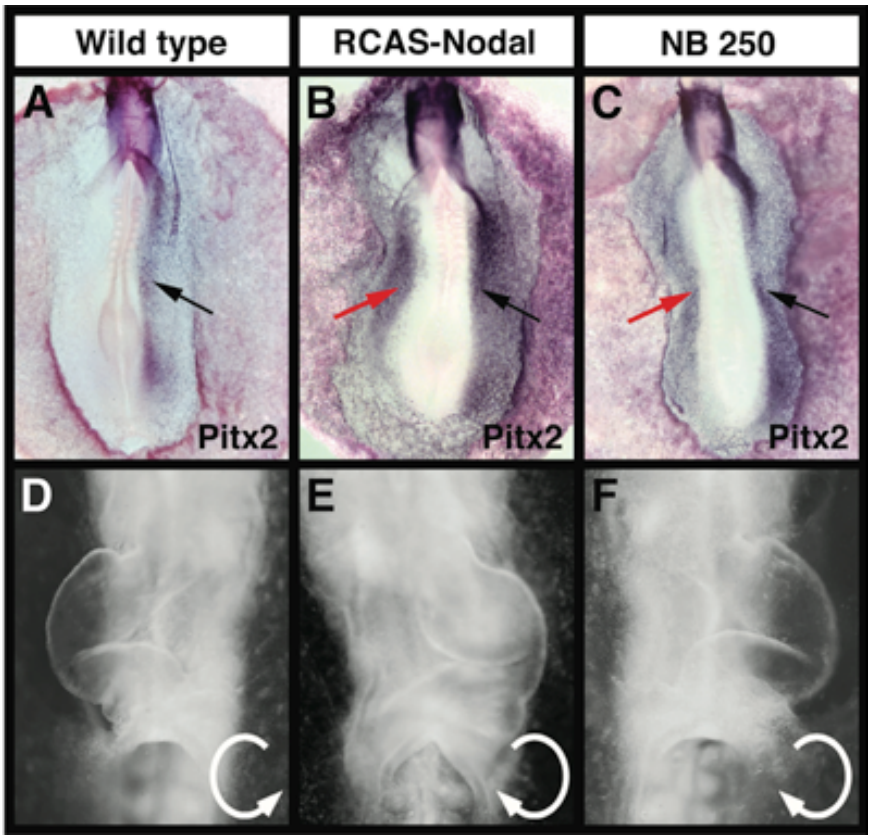

Figure 2-4: In vivo development by NB250 using developing chick embryos. A) *Pitx2* transcripts are detected along the entire left side of the lateral plate mesoderm (arrow). B) Ectopic expression of Nodal on the right side of chick embryos inducing *Pitx2* transcripts on the right side of the lateral plate mesoderm (red arrow). C) A bead soaked with NB250 inducing ectopic *Pitx2* transcripts along the right lateral plate mesoderm (red arrow) D) Wild-type chick embryo develops with a rightward heart looping (arrow). Both E) Nodal and F) NB250 reverse heart looping in a leftward orientation (arrows).

Based on these results, it can be concluded that chimeric ligand NB250 is functionally identical to Nodal. Our assays have shown conclusively that NB250 signals via the Activin pathway used by Nodal, exhibits Cripto dependency like Nodal, and is able to achieve the same effects on heart looping *in vivo* as Nodal.

NB2 Chimeras can induce chondrogenesis

NB2 chimeras are composed of segments derived from BMP2 and Nodal. BMP2 and Activin have been observed to play a role in chondrogenesis, whereas Nodal has no known implications in this process. However, Nodal shares its signalling pathway with Activin, thus we inferred that it may also induce chondrogenesis. Therefore, we decided to test Nodal and the NB2 chimeras for their chondrogenic potential in collaboration with the Belmonte Lab (Salk Institute).

In order to determine the potential of the Nodal ligands to induce chondrogenesis, real time PCR analyses were performed. The results show that Nodal, NB250 and NB260 induce the expression of chondrogenic markers Col II, Sox9, and Aggrecan at very similar levels (Figure 2-5).

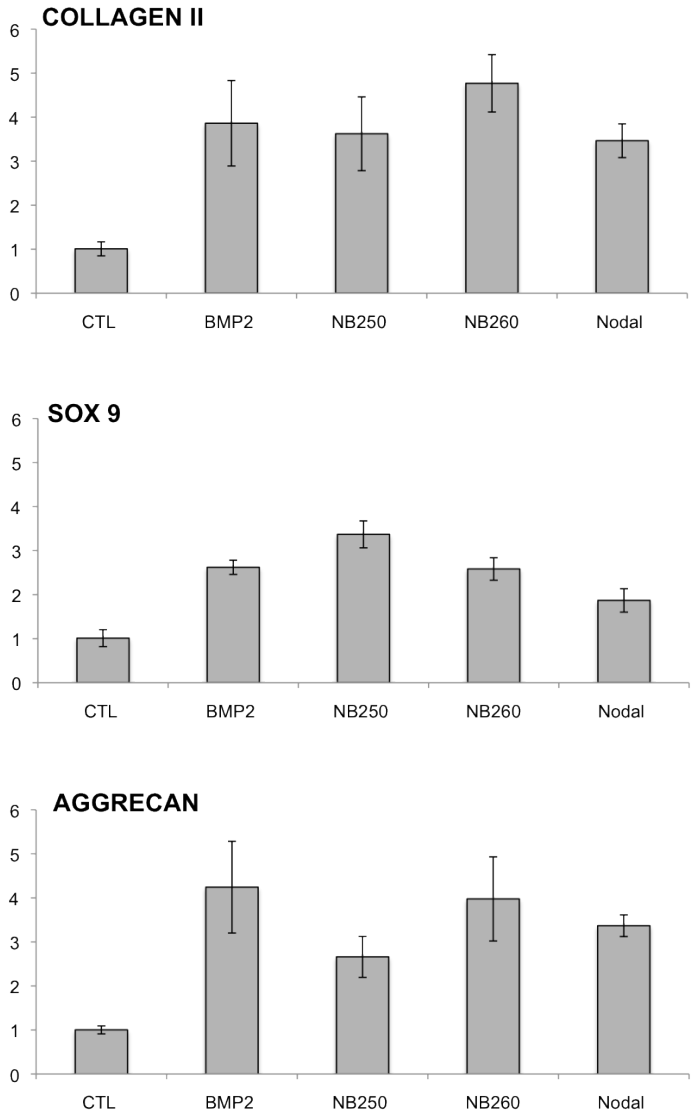

Figure 2-5: Real-time PCR analysis of selected chondrogenic markers after the cells were cultured for 14 days in complete chodrogenic medium containing the different ligands. Gene expression is shown as fold change compared to cells cultured in incomplete chodrogenic medium (CTL).

To further evaluate the chondrogenic potential of the chimeras, we performed inmunocytochemistry assays on cells grown in monolayer and differentiated for 4 weeks. Monolayer cultured cells treated with NB250 and NB260 clearly exhibit an increase in the expression of type II Collagen, which

develops into a dense filamentous matrix network that is deposited over the cells (Figure 2-6A).

Additionally, we used a cell pellet culture model to mimic the cellular condensation process occurring in normal limb development. After 6 weeks of culture, pellets supplemented with NB250, NB260, or BMP2 achieved a cartilage-like appearance with a white shiny look resembling cartilage tissue and showed a marked increase in size compared to cell pellets grown in incomplete chondrogenic medium (CLT) (Figure 2-6B). Taken together, these results suggest that both NB250 and NB260 have a strong potential to induce chondrogenesis.

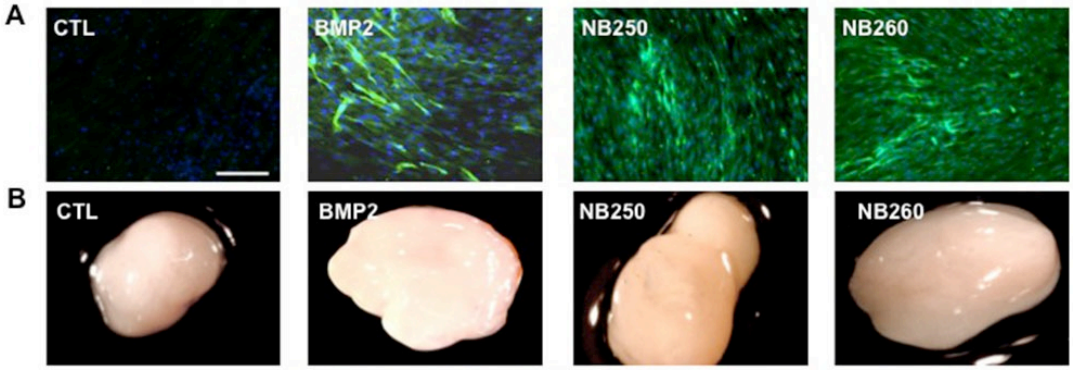

Figure 2-6: NB250 and NB260 induce the formation of cartilage-like tissue. A) Immunochemistry assays of monolayer cells treated with NB260 for 4 weeks. Type II Collagen is stained green. B) hASCs cultured in a pellet system treated with Nodal ligands (NB250 and NB260), BMP2, or grown in incomplete chondrogenic medium as negative control (CTL). Scale bar: 65 mm for A.

The results obtained from these studies indicate that a number of Nodal chimeras exhibit similar signaling capabilities as Nodal and may have been endowed with enhanced properties. I decided to focus on NB250 due to its BMP2 makeup, which may confer rigidity to the ligand, and due to the fact that

its production is the most efficient out of all the NB2 chimeras tested. Furthermore, this chimera was the least Nodal-like out of the ones tested (composed of only 3 Nodal segments) yet it mimics Nodal *in vivo* and has chondrogenic properties. Therefore, the structure of this ligand may aid in determining the key regions of the protein involved in Nodal signaling and chondrogenic activities. Finally, the rigidity of NB250 may aid in the formation of its signaling complex, which would facilitate its study.

NB250 Crystallization

NB250 was resuspended in water at a concentration of 10 mg/ml and crystallization trials with several commercial screening kits including Crystal Screen, Crystal Screen 2 (Hampton Research), Wizard Screens I and II (Emerald BioStructures), PEG/ION and Nextal Classics suite (Qiagen) were conducted using the Mosquito crystallization robot (ttp labtech, Cambridge, MA). These screens yielded several crystallization hits, which were subsequently optimized. The final crystal (Figure 2-7) was obtained using the hanging drop vapor diffusion method, in which 1 µl of 10 mg/ml protein was mixed with 1 µl of a reservoir solution of 0.2M NaCl, 0.1 M Na acetate pH 4.6, 30% 2-Methyl-2,4-pentanediol and incubated at 15 °C. Crystals were frozen in liquid N_2 using a cryoprotectant comprised of the original reservoir solution supplemented with 15% (v/v) glycerol. Diffraction data at a resolution of 1.9 Å were collected at the Stanford Synchrotron Radiation Lightsource (SSRL) using beamline 11-1.

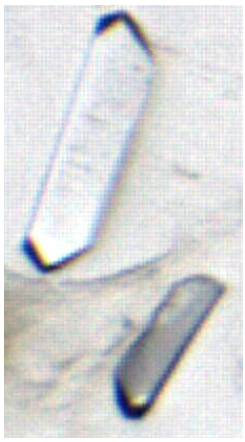

Figure 2-7: NB250 crystals used for x-ray analysis.

The space group of NB250 was found to be R3. Data were processed using XDS software (8) and the structure was solved using molecular replacement with BMP2 as a model. Model building was done in COOT version 0.6.2 (9). Refinement of the structure was completed using REFMAC, version 5.5.0109 (10) to R and R_{free} values of 0.18 and 0.21, respectively. The final data processing and refinement statistics are listed in Table 2-1. All structure figures were generated using PyMOL (version 1.3; Schrödinger) (11) and Molscript version 2.1.2 (12).

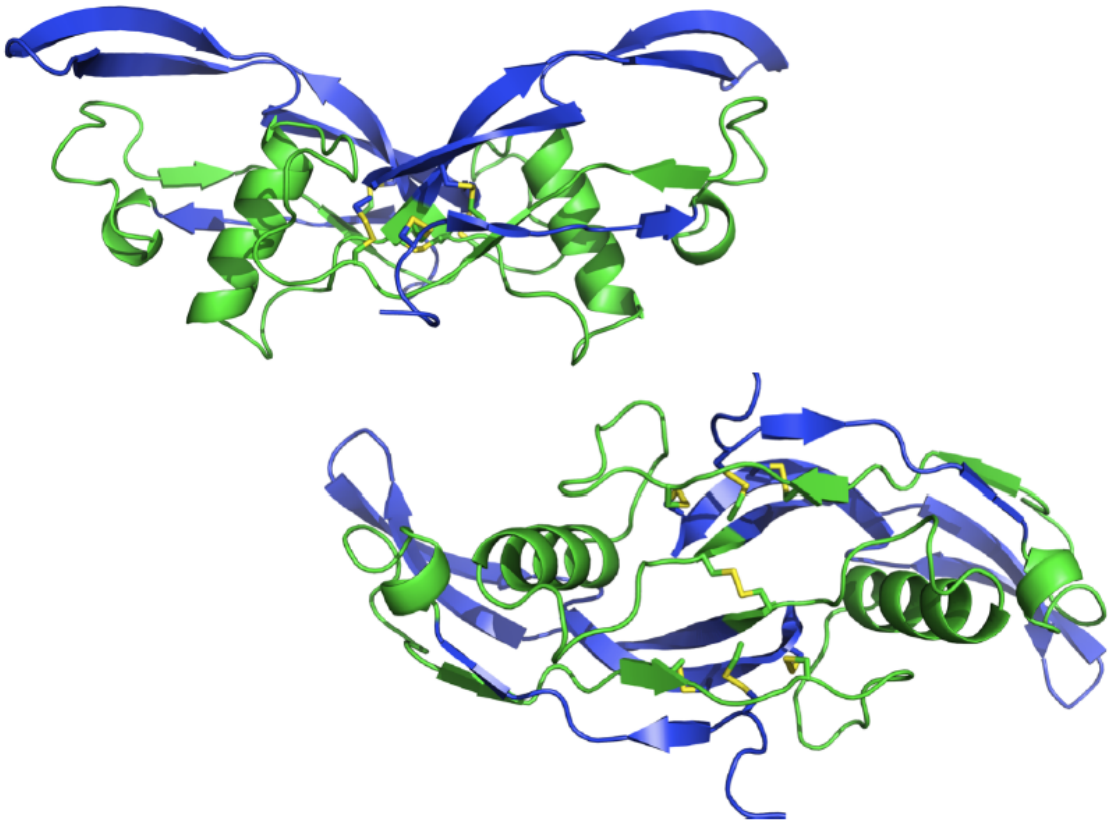

```
NB250          1  QAKHKQRKRLKSSCKRHPLYVDFNLIGWGSWIIYPKQYNAYRCEGECPNPVGEEFHPTNH 60
              61  AYIQSLLKRYQPHRVPSTCCVPTELSAISMLYLDENEKVVLKNYQDMVVEGCGCR 115
```

Figure 2-8: Structure and amino acid sequence of NB250. Top: front view. Bottom: 90° rotation. Nodal segments are colored green, BMP2 segments are colored purple.

Table 2-1: Data processing and refinement statistics for NB250. Numbers in parentheses correspond to the highest resolution shell.

NB250 X-ray Data Collection and Refinement Statistics	
Observed Reflections	128,923
Unique Reflections	13,314
Resolution Range (Å)	63.1-1.91 (1.96-1.91)
Mean (I/σ)	41.95 (3.72)
Completeness (%)	99.2 (90.4)
R_{merge}	0.033 (0.40)
R_{cryst}	0.18
R_{free}	0.21

Structure of NB250 closely resembles that of BMP2

Similar to BMP2, the NB250 monomer has 7 cysteine residues. These residues allow the monomer to form three intra-disulfide bonds (Cys14/Cys80, Cys43/Cys112, and Cys47/Cys114) and one inter-disulfide bond, which is formed between the Cys79 of each monomer. These disulfide bonds, along with alpha helix a1, formed by the region between residues Asn59 and Tyr70, comprise the core of the protein. The overall architecture of the dimer is similar to that of BMP2, dictated by these disulfide bonds (cysteine knot motif) coupled with four anti-parallel β-strands extending outward from the core, giving it a spread wing shape (Figure 2-8). The pre-helix loop, helix a1, and beta sheet β2 are entirely composed of Nodal segments depicted in green in figure 2-8, whereas beta sheets β1, β3, and β4 are composed by residues belonging to the BMP2 segments depicted in purple in the same figure. When NB250 and BMP2 are superimposed based on their shared sections 1B, 5B,

and 6B, the Cα RMSD is 0.629 Å (Figure 2-9). As expected, the regions of highest structural discrepancy lie in the 2N3N4N region of NB250.

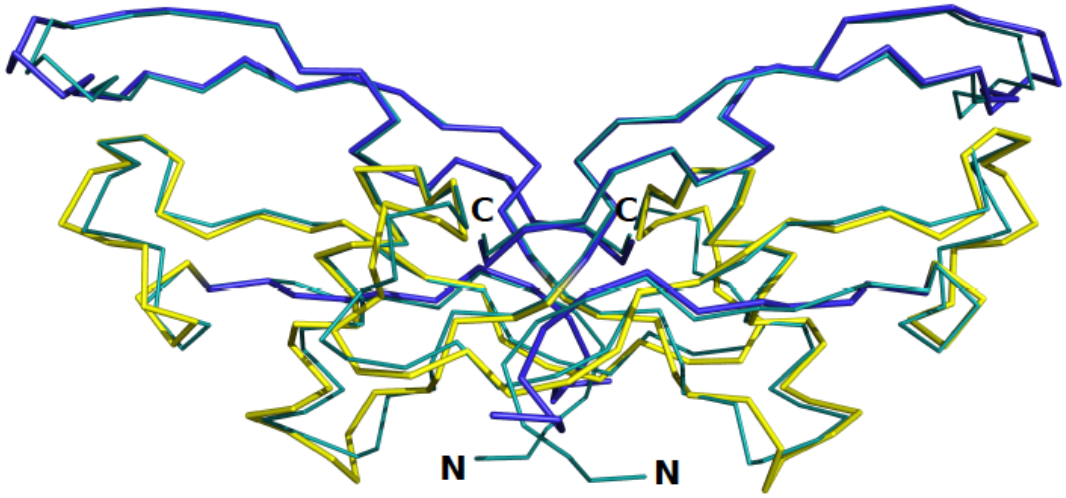

Figure 2-9: Cα alignment of BMP2 (thin line, cyan) and NB250 (thicker line, yellow/purple). NB250's BMP2 segments are depicted in yellow, and its Nodal segments are depicted in purple.

NB2 chimeras require sections 2N, 3N, and 4N to retain Nodal functions

Previous studies suggest that sections 2N, 3N, and 4N are relevant for Cripto dependency because they encompass structural elements that have been proposed to play a role in Nodal's inability to bind ALK4 in the absence of Cripto (14). Therefore, it can be inferred that in order to retain Nodal functionality the minimal required Nodal segmental sequence is 2N3N4N, with NB250 (BNNNBB) being a "minimalistic" chimera with Nodal functionality.

NB250 has been shown to be functionally indistinguishable from Nodal. However, its sequence is one half Nodal and one half BMP2, yet it clearly exhibits the same extended fold as BMP2. Interestingly, NB250 does not signal through the Smad 1/5/8 pathway used by BMP2, yet it is able to induce

chondrogenesis. Nodal and BMP2 share the same type II receptor -ActRII- and, despite NB250's chimeric sequence, the binding epitope for its type II receptor mostly resembles that of BMP2. Nodal signaling is regulated by Cripto, which binds to Nodal via its EGF-like domain, and ALK4 via its CFC domain (15). It is therefore not surprising that substituting BMP2's type II receptor binding epitope in Nodal, as is the case in NB250, will not disrupt Nodal function, given that the region where Cripto is predicted to bind is conserved in NB250.

Residue changes in NB250's receptor binding epitopes determine its enhanced affinity for ActrRII and its inability to bind BMPRIa

Having solved the structure of NB250, I sought to compare this chimera's type I and type II receptor binding epitopes with those of its parental ligand BMP2. The key residue responsible for the potential differences between BMP2 and NB250 in type II receptor binding as well as the key residues that could possibly modify type I receptor binding were identified by superimposing the NB250 structure onto the BMP2/BMPRIa/ActRII ternary complex (13) (Figures 2-10 and 2-11).

Affinity studies of NB250 binding to ActrII indicate that this ligand has two times higher affinity for its type II receptor than BMP2, with corresponding Kd values equaling 15nM and 37nM respectively. This observation may be explained by a residue change in NB250's ActRII binding epitope that could slightly enhance this chimera's affinity for its type II receptor.

Previous studies have identified Ala34, Pro35, Ser88, Met89, and Leu90 in BMP2 as being implicated in the formation of the hydrophobic interface required for ActRII binding via its hydrophobic residues Phe83, Phe42, and Trp60 (13). NB250 shares these residues with BMP2 with the exception of Ala34, which is substituted by Tyr in NB250. After aligning the NB250 structure with the BMP2/BMPRIa/ActRII ternary complex (Figure 2-10), it can be seen that the aromatic side chain in Tyrosine can form pi-stacking interactions with ActRII's Phe83, which could potentially enhance NB250's affinity for its type II receptor.

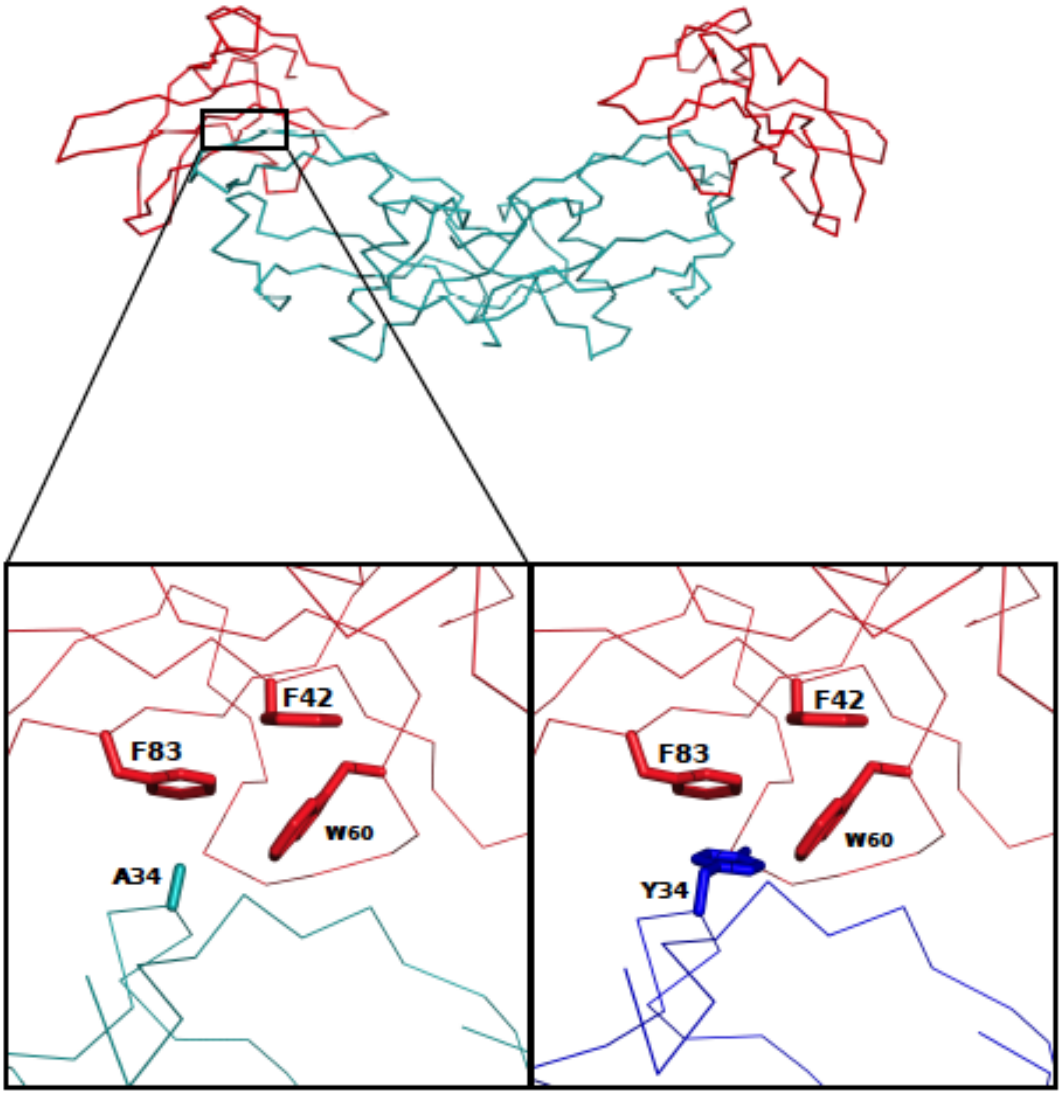

Figure 2-10: Key residues responsible for the increased affinity to type II receptor in NB250. Top image: front view of the BMP2 (cyan)/ActRII (red) complex. The key region of the BMP2/ActRII interface is boxed. Bottom left: close-up of this region showing the original BMP2 Ala34 residue (cyan) and ActRII's Phe83, Phe42 and Trp60 residues (red). Bottom right: same region, with BMP2 replaced by NB250 (purple) showing the substitution of the non-interacting BMP2 Ala34 residue with the interacting Tyr34 residue from NB250.

Failure to observe BMP2-like signaling through Smad1/5/8 suggests that NB250 has a decreased affinity for the canonical BMP2 type I receptor BMPRIa. This may be caused by disruptive residue changes that are a

product of NB250's chimeric makeup. When the structure of NB250 is aligned to BMP2 of the BMP2/BMPRIa/ActRII complex, four residues that have been found to play a role in the formation of the two BMP2 hydrophobic pockets required for receptor binding (13) are different: Val26 in BMP2 is an Ile in NB250, Phe49 is an Asp, and Ile62 as well as Val70 have been substituted for Tyr. Out of these substitutions, the most detrimental appears to be Phe49Asp, due to the fact that Phe49 inserts tightly to the hydrophobic pocket formed by BMPRIa's Ile62, Ile99, and Phe60 (Figure 2-11) and the change of a hydrophobic residue for a polar residue most likely disrupts this interaction, severely hindering BMPRIa's ability to bind to NB250.

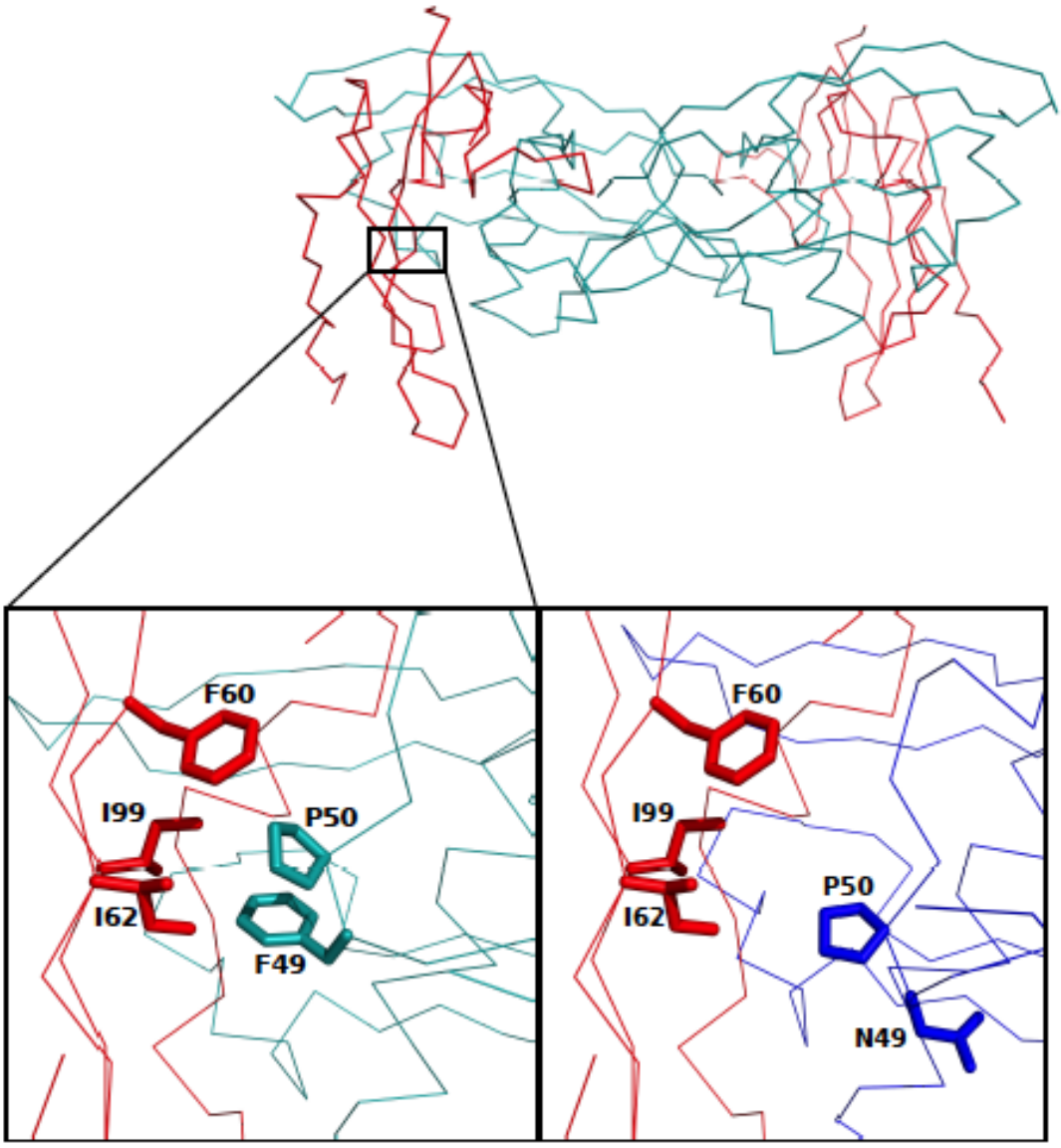

Figure 2-11: Key residues responsible for the decreased affinity to type I receptor in NB250. Top image: front view of the BMP2 (cyan)/BMPRIa (red) complex. The key region of the BMP2/BMPRIa interface is boxed. Bottom left: close-up of this region showing the original BMP2 Phe49 residue (cyan) and BMPRIa's Ile62, Ile99 and Phe60 residues (red). Bottom right: same region, with BMP2 replaced by NB250 (purple) showing the substitution of the BMP2 Phe49 residue with the Asn49 residue from NB250.

The lack of signaling through the main BMP2 pathway makes it difficult to explain the chondrogenic properties observed for NB250. Nonetheless,

previous studies have shown that the Activin signaling pathway, used by Nodal and the NB2 chimeras studied, also plays a role in chondrogenesis. Indeed, there is a case to be made for a novel role of Nodal in chondrogenesis, given that NB250 is able to mimic Nodal *in vivo* and drive chondrogenic differentiation, and that Nodal, NB250, and NB260 are able to induce chondrogenic markers. Furthermore, the fact that NB260 is able to induce chondrogenesis at levels superior to those seen in BMP2 suggest that Nodal may play a synergistic role with other BMPs in chondrogenesis, perhaps by creating a signaling complex that is capable of crosstalk with other signaling pathways involved in this process.

The structure of NB250 has shown that this chimeric ligand is structurally very similar to BMP2, having rigidity similar to this ligand. Combining this finding with the fact that NB250 appears to be indistinguishable from Nodal in its signaling and effects on left-right heart looping in chick embryos, it can be concluded that Nodal itself adopts a BMP2-like fold.

Furthermore, structural analysis of this chimeric ligand suggests that NB250's distinct affinities for its receptors can be attributed to changes in its receptor binding epitopes. Finally, the fact that NB250 is able to mimic Nodal *in vivo*, utilizes the same signaling pathway as Nodal, and has chondrogenic properties suggest a new role for Nodal in chondrogenesis and presents NB250 as a viable, easier to produce, Nodal substitute.

This chapter is currently being prepared for submission for publication of the material. Esquivies L, Blackler A, Peran M, Rodriguez-Esteban C,

Izpisua Belmonte C, Gray P, Booker E, Ahn C, Kwiatkowski W, Choe S. “Designer Nodal/BMP2 chimeras mimic Nodal signaling, promote chondrogenesis, and reveal a BMP2-like structure”. The dissertation author was the primary author of this paper.

References

1. Zhou X, Sasaki H, Lowe L, Hogan BL, Kuehn MR (1993) Nodal is a novel TGF-β-like gene expressed in the mouse node during gastrulation. *Nature* **361**: 543-547.

2. Conlon FL, Lyons KM, Takaesu N, Barth KS, Kispert A, Hermann B, Robertson EJ (1994) A primary requirement for nodal in the formation and maintenance of the primitive streak in the mouse. *Development* **120**: 1919-1928.

3. Tsuchida K, Nakatani M, Uezumi A, Murakami T, Cui X (2008) Signal transduction pathway through activin receptors as a therapeutic target of musculoskeletal diseases and cancer. *Endocr. J.* **55**: 11-21.

4. Chea HK, Wright CV, Swalla BJ (2005) Nodal Signaling and the Evolution of Deuterostome Gastrulation. *Developmental Dynamics* **234**: 269-278.

5. Montero J, Lorda-Diez C, Gañan Y, Macias D, Hurle J (2008) Activin/TGFbeta and BMP crosstalk determines digit chondrogenesis. *Developmental biology* **321**: 343-356.

6. Schier A (2009) Nodal morphogens. *Cold Spring Harbor perspectives in biology* **1**:a003459.

7. Ryan AK, Blumberg B, Rodriguez-Esteban C, Yonei-Tamura S, Tamura K, Tsukui T, de la Peña J, Sabbagh W, Greenwald J, Choe S, Norris DP, Robertson EJ, Evans RM, Rosenfeld MG, Izpisua Belmonte JC (1998) Pitx2 determines left-right asymmetry of internal organs in vertebrates. *Nature* **394**: 545-551.

8. Kabsch W (2010) XDS*. Acta Crystallogr D Biol Crystallogr* **66(Pt 2)**: 125–132.

9. Emsley P, Lohkamp B, Scott WG, Cowtan K (2010) Features and development of Coot. *Acta Crstallogr D Biol Crsytallogr* **66(Pt 4):** 486-501.

10. Murshudov GN, Vagin AA, Dodson EJ (1997) Refinement of macromolecular structures by the maximum-likelihood method. *Acta Crystallogr. D. Biol. Crystallogr.* **53(Pt 3):** 240-255.

11. The PyMOL Molecular Graphics System, Version 1.3 Schrödinger, LLC.

12. Kraulis PJ (1991) MOLSCRIPT: A Program to Produce Both Detailed and Schematic Plots of Protein Structures. *Journal of Applied Crystallography* **24**: 946-950.

13. Allendorph GP, Vale WW, Choe S (2006) Structure of the ternary signaling complex of a TGF-b family member. *Proc. Natl. Acad. Sci. USA* **103**: 7643-7648.

14. Romano V, Raimondo D, Calvanese L, D'Auria G, Tramontano A, Falcigno L (2012) Toward a better understanding of the interaction between TGF-b family members and their ALK receptors. *J Mol. Model*. **18**: 3617-3625.

15. Yeo C, Whitman M (2001) Nodal signals to Smads through Cripto-dependent and Cripto-independent mechanisms. *Mol Cell* **7**: 949-957.

Chapter 3. Structural studies of an Activin/BMP2 chimera that is functionally identical to Activin and a Noggin-insensitive Activin/BMP2 chimera that strongly accelerates osteogenic differentiation.

Introduction

The study of Activin A and its signaling complexes has been hindered by the difficulty to generate this ligand in quantities suitable for structural studies. Even though this protein has been successfully produced using stably (1) and transiently (2) transfected cell lines, the cost and time required to generate Activin A makes these techniques inadequate for use in structural investigations. Furthermore, these expression systems are not the most advantageous for studying Activin variants given the time required for producing the variants as well as the protein yields obtained using these methods.

In order to circumvent these obstacles, Allendorph et al. (3) employed the RASCH strategy to develop a set of chimeric ligands combining Activin and BMP2 segments. Among these chimeras, AB208 was shown to mimic Activin A in all functional tests (3). In an effort to determine whether this chimera retained the structure and flexibility of its parental ligand Activin A, the structure of AB208 was elucidated.

Additionally, it has been shown that other members of the chimeric AB2 ligand library exhibit osteogenic activity that is markedly superior to BMP2 (4). One such chimera, termed AB204, has been shown to increase osteogenic markers in proteoblastic cells 3-8 fold higher than its parental ligand BMP2. Furthermore, AB204 is capable of healing tibial and calvarial critical size defects, and exhibits insensitivity to Noggin, a known BMP

inhibitor. In order to better understand the novel properties exhibited by this chimera, the crystal structure of AB204 was elucidated.

AB208 crystallization

AB208 (chimeric sequence BAAAAA) was resuspended in water to a concentration of 10 mg/ml, and crystallization trials were conducted using the hanging drop vapor diffusion method with several commercial screening kits: Crystal Screen, Crystal Screen 2 (Hampton Research), Wizard Screens I and II (Emerald BioStructures), PEG/ION and Nextal Classics suite (Qiagen) using the Mosquito crystallization robot (ttp labtech, Cambridge, MA). Crystallization hits obtained from these screens were optimized.

The protein crystallized in the I222 space group, producing orthorhombic crystals (Figure 3-1). The crystals used for x-ray analysis were obtained by combining 1 µl of protein at 10 mg/ml with 1 µl of a crystallization condition composed of 20 or 25% Ethanol, 0.1 M Tris 8.5, and incubating this drop at 15 °C using the hanging drop vapor diffusion method. The crystals were frozen in liquid N_2, with 15% Glycerol used as cryoprotectant.

Figure 3-1: AB208 crystals used for x-ray analysis.

Thirty crystals were analyzed at SSRL beamline 11-1, diffracting at resolutions between 5.0-3.3 Å. Data were processed using XDS software (5) and the structure was solved using molecular replacement with Activin A as a model. Model building was done in COOT version 0.6.2 (6). Refinement of the structure was completed using REFMAC, version 5.5.0109 (7) to R and R_{free} values of 0.28 and 0.37, respectively. All structure figures were generated using PyMOL (8). Processing and refinement statistics are presented in table 3-1.

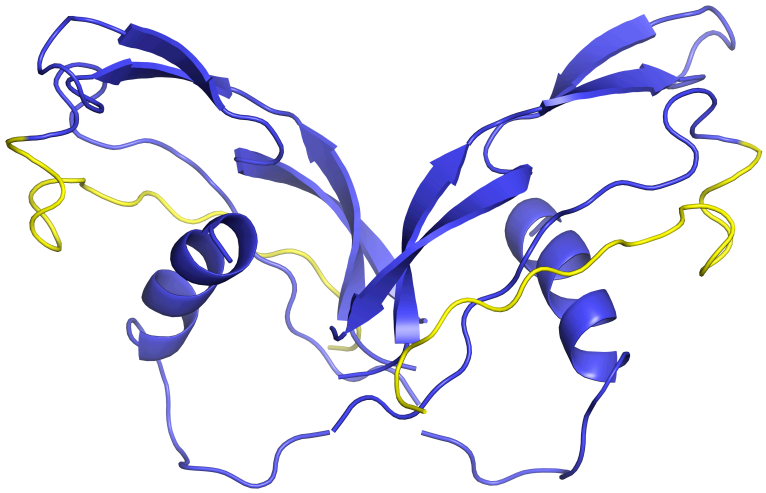

```
                                1                                2                                3
BMP2          1  QAKHKQRKRLKSSCKRHPLYVDFSDVGWNDWIVAPPGYHAFYCHGECPFPLADHLNSTNH 60
Activin-βA    1  --GLECDGKVNICCKKQ-FFVSFKDIGWNDWIIAPSGYHANYCEGECPSHIAGTSGSS-L 56
AB208         1  QAKHKQRKRLKSSCKRHPLYVDFSDVGWNDWIIAPSGYHANYCEGECPFPLADHLNSTNH 60

BMP2         61  AIVQTLVN----SVNSKIP--KACCVPTELSAISMLYLDENEKVVLKNYQDMVVEGCGCR 114
Activin-βA   57  SFHSTVINHYRMRGHSPFANLKSCCVPTKLRPMSMLYYDDGQNIIKKDIQNMIVEECGCS 116
AB208        61  AIVQTLVN----SVNSKIP--KACCVPTKLRPMSMLYYDDGQNIIKKDIQNMIVEECGCS 114
                                 4                5                6
```

Figure 3-2: Structure and sequence of AB208 (BAAAAA), with sequence alignment of BMP2 (yellow) and Activin A (purple) used to make the chimeric ligand.

Table 3-1: Data processing and refinement statistics for AB208. Numbers in parentheses correspond to the highest resolution shell.

AB208 X-ray Data Collection and Refinement Statistics	
Observed Reflections	41,655
Unique Reflections	6,561
Resolution Range (Å)	61.17-3.30 (3.34-3.23)
Mean (I/σ)	4.51 (3.1)
Completeness (%)	98.4 (98)
R_{merge}	0.039 (0.43)
R_{cryst}	0.28
R_{free}	0.37

Discussion

It should be noted that the building of some sections of the model (mainly the helix and pre-helix loops) proved problematic due to the resolution of the data and the high level of flexibility of the chimeric ligand (Figure 3-2). Nonetheless, this structure serves as a starting point for determining the general structural features of AB208.

AB208 clearly resembles Activin A, which is to be expected given that AB208 is 83% Activin A, with only the first part of finger 1 derived from BMP2 (Figure 3-2). The main features of a mature TGF-β ligand can be seen, such as the "spread wing" conformation formed by the beta sheets, the cysteine knot motif comprised of interdisulfide bonds Cys43/Cys116, Cys47/Cys118, and Cys14/Cys84, and an interdisulfide bond between the Cys83 of each monomer.

Furthermore, a Cα alignment of Activin A and AB208 (Figure 3-3) yields a RMSD of 0.7 Å, indicating a significant structural similarity between these two ligands.

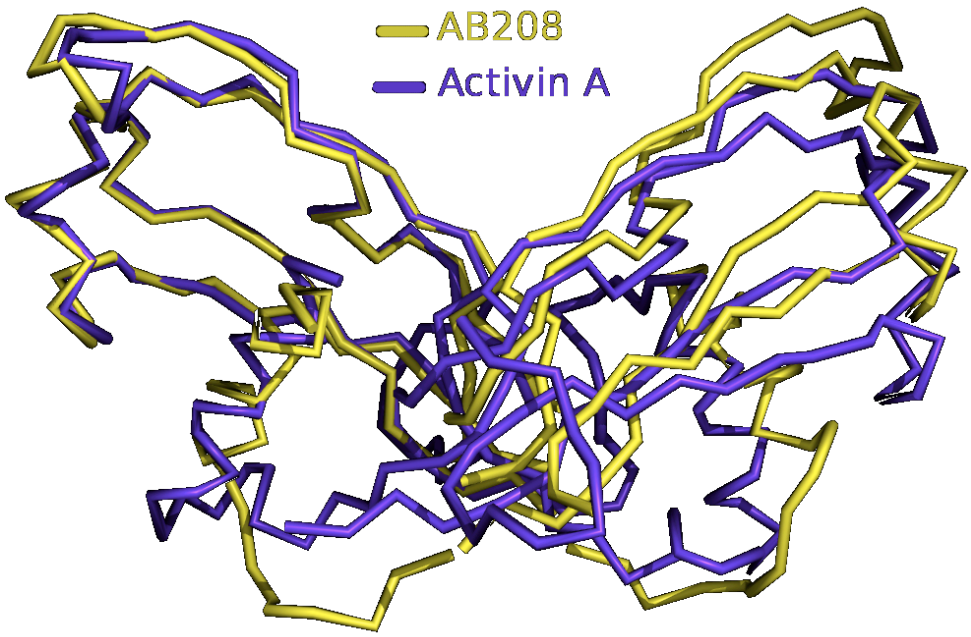

Figure 3-3: Cα alignment of AB208 and Activin A.

Functional studies have shown that AB208 has the same receptor binding profile as Activin A, given that it can bind type II receptor ActRII with an affinity comparable to that of Activin A. Indeed, binding assays indicate that Activin A binds ActRII-ECD with an affinity of 0.203 nM, whereas AB208 binds this receptor with an affinity of 0.344 nM (3). Furthermore, this chimeric ligand has also been shown to be inhibited by Cripto, as Smad2 signaling assays show that AB208 and Activin signaling is decreased by ~68% and ~57% respectively when these ligands interact with Cripto (3).

The AB208 structure suggests that this ligand does not suffer any major changes from Activin A in its structure and flexibility due to the substitution of part of its sequence with BMP2 sequence. Moreover, and just as importantly, AB208's chimeric composition has not introduced structural elements that

could distort its binding affinities to the receptors used by Activin A as well as its inhibitors.

Therefore, and based on the functional and structural data available, it can be concluded that AB208 is a strong candidate for a viable Activin A substitute in the study of signaling complexes and biological processes in which this ligand plays a role.

AB204 crystallization and structure

AB204 was resuspended in 10 mM Na Acetate pH 4 at 10 mg/ml. An initial crystallization screen was conducted as previously described for AB208. Crystallization trials yielded several hits, which were subsequently optimized.

The best diffracting crystal was obtained using the hanging drop vapor diffusion method, in which 1 µl of protein was mixed with 2 µl of a reservoir solution of .2 M $LiSO_4$, .1 M Tris 8.5, and 30% PEG 4,000 and incubated at 15 °C (Figure 3-4).

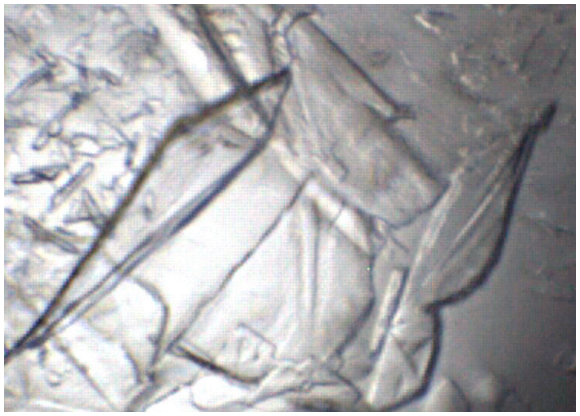

Figure 3-4: AB204 crystals used for x-ray analysis.

Diffraction data were collected in house using a Micromax-007HF X-ray generator (Rigaku, Tokyo, Japan) to a resolution of 2.3 Å. The space group of AB204 was found to be $P3_121$. Data were processed using XDS software (5) and the structure was solved using molecular replacement with BMP2 as a model. Model building was done in COOT version 0.6.2 (6). Refinement of the structure was completed using REFMAC, version 5.5.0109 (7) to R and R_{free} values of 0.25 and 0.28, respectively. All structure figures were generated using PyMOL (8) and Molscript version 2.1.2 (9).

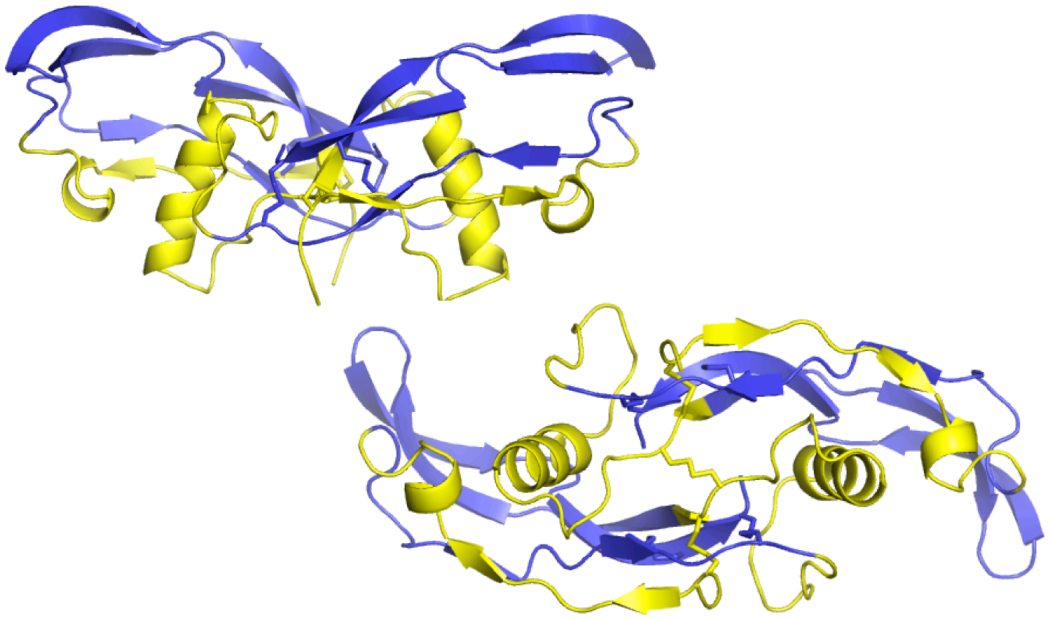

Figure 3-5: Structure of AB204. Top: front view, bottom: 90° rotation. BMP2 segments are yellow, Activin A segments are purple.

Table 3-2: Data processing and refinement statistics for AB204. Numbers in parentheses correspond to the highest resolution shell.

AB204 X-ray Data Collection and Refinement Statistics	
Observed Reflections	43,942
Unique Reflections	5,351
Resolution Range (Å)	28.25-2.14 (2.21-2.14)
Mean (I/σ)	33.18 (5.41)
Completeness (%)	96.41 (79.22)
R_{merge}	0.055 (0.248)
R_{cryst}	0.252
R_{free}	0.284

Discussion

The structure of AB204 conforms to the general structural TGF-β ligand pattern (Figure 3-5). Similar to BMP2, the AB204 monomer has a cysteine knot motif comprised of three intra-disulfide bonds (between Cys47/Cys113, Cys14/Cys79, and Cys43/Cys111) and one inter-disulfide bond formed between the Cys78 of each monomer. Three disulfide bonds of the cysteine knot, along with a short alpha helix (residues Asn59 through Val70), encompass the core of the protein. Each AB204 monomer has 4 antiparallel-β strands that form 2 antiparallel β-sheets (fingers 1 and 2) extending outward from the cysteine knot core, giving it an appearance of the spread-wing shape of a butterfly.

The majority of the type I receptor binding epitope of AB204 (pre-helix loop, helix, and the bottom part of finger 1) is composed of BMP2 residues (segments 1, 3, and 4 of AB204, Figure 3-6A). On the other hand, the binding epitope for type II receptors (top half of finger 1 as well as the entire finger 2) comprises residues belonging to Activin A (segments 2, 5, and 6, Figure 3-6A). The superposition of the BMP2 and AB204 structures based on their shared segments shows a RMSD of 0.67 Angstrom (Figure 3-6B). This similarity suggests that AB204 adopts a spread fold characteristic of BMP ligands rather than a compact, more flexible Activin fold.

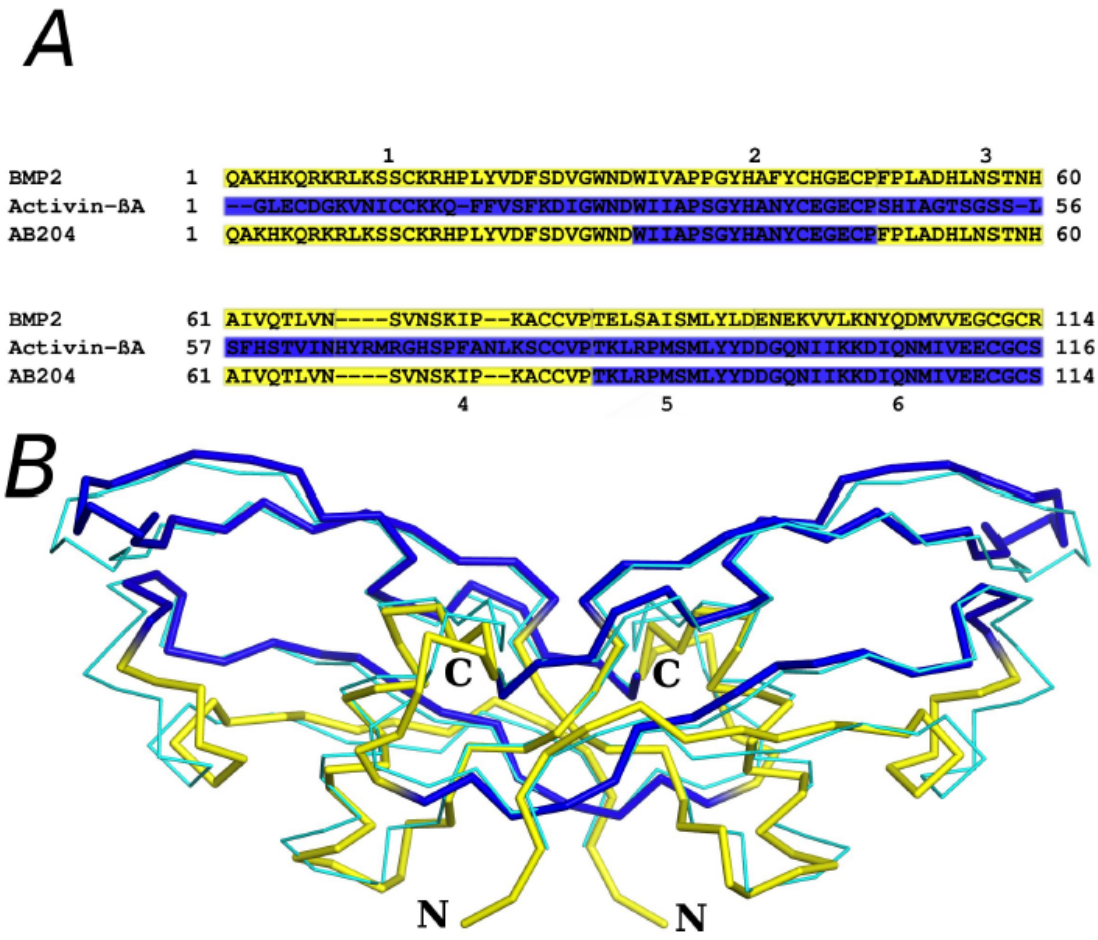

Figure 3-6: A) Sequence alignment of BMP2 (cyan), Activin A (purple) and AB204 (cyan and purple). Six segments are depicted to show AB204's composition. B) Superposition of AB204 and BMP2. BMP2 is depicted with a thin cyan line. AB204 is depicted with a thicker line with its BMP2 segments in cyan and its Activin segments in purple. N and C terminals are indicated.

Studies have shown that AB204 exhibits enhanced osteogenic properties that surpass those seen for BMP2. Furthermore, this chimeric ligand has been found to be insensitive to Noggin and to have a ~100 fold increase in affinity to the ActRII receptor compared to BMP2. Therefore, I decided to determine the structural features that conferred these novel properties to this ligand.

The key residues responsible for the differences observed in type I receptor binding were identified by superposing AB204 onto the BMP2/BMPRIA/ActRII ternary complex (10). Additionally, the key residues responsible for AB204's Noggin-insensitivity were determined by overlaying AB204 on BMP7 of the Noggin/BMP7 complex (11). Interestingly, this overlay indicates that a residue that plays a key role in the Noggin-binding epitope of BMP7 is missing in AB204.

The structure of AB204 shown indicates that it adopts the overall architecture of BMP family ligands, even though AB204 shares half of its amino acid sequence with Activin. Activin, unlike BMPs, displays a high level of plasticity, with flexible wings and a disordered type I binding epitope (12). AB204 shares part of finger 1 and finger 2 with Activin. These are the most rigid parts of Activin and play a role in forming two conserved β-sheets of TGF-β superfamily ligands. Therefore it is not entirely surprising that AB204 adopts a BMP2 conformation, given that its Activin component is derived from the most rigid parts of this ligand.

AB204's binding epitope for type II receptor, which is positioned near the fingertips of the ligand, is derived from Activin. Therefore, AB204's and Activin's affinities to their type II receptor, ActRII, are practically the same, having Kd values 0.38 and 0.20, respectively (3).

In addition, AB204's type I receptor binding epitope is mostly derived from BMP2. Based on the BMP2/BMPRIA/ActRII complex structure (10) it is evident that there is one important contact between finger 2, which has the

Activin sequence in AB204, and BMPRIA. Tyr103 of BMP2 creates a strong hydrogen bond to Asp84 of BMPRIA, aided by additional Pi stacking interactions between Tyr103 of BMP2 and Phe85 of BMPRIA. Since Tyr103 is replaced by Ile103 in AB204, the aforementioned stable interactions at the AB204/BMPRIA interface are absent (Figure 3-7), which explains the observed reduction in affinity for the type I receptor.

Based on these findings, it can be hypothesized that the extended retention of the bound type II receptors in the complex with AB204 can result in increased phosphorylation of weakly bound type I receptors, thus prolonging and increasing the resulting signaling level.

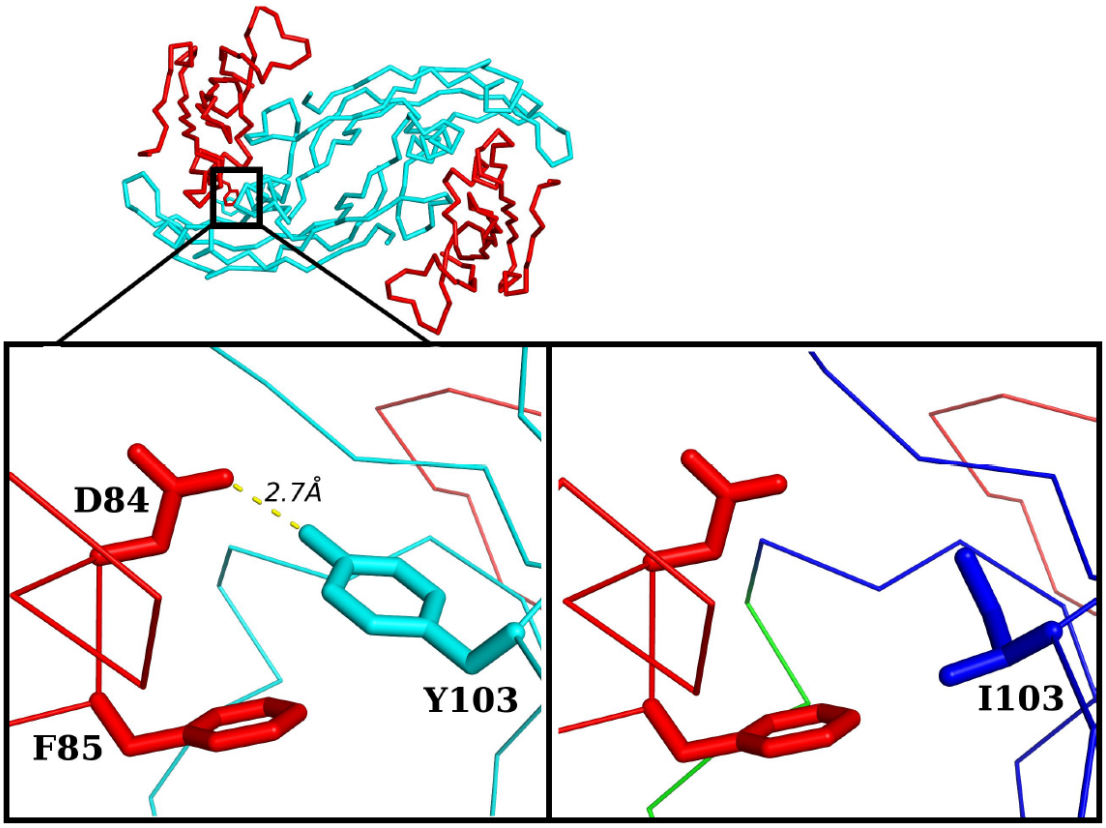

Figure 3-7: Key residues responsible for the diminished affinity to type I receptor in AB204. Top image: top view of the BMP2 (cyan)/BMPRIA (red) complex. The key region of the BMP2/BMPRIA interface is boxed. Bottom left: close-up of this region showing critical interactions between BMP2's Tyr103 residue (cyan) and BMPRIA's Asp84 and Phe85 residues (grey). Bottom right: same region, with BMP2 replaced by AB204 (purple) showing the substitution of the interacting BMP2 Tyr103 residue with the non-interacting Ile103 residue from AB204.

The Noggin/BMP7 complex structure (11) clearly shows that Noggin binding to BMPs blocks the ligand's access to its Type I and Type II receptors. Using the AB204 structure, it was determined that these epitopes in AB204 are different enough to impede Noggin binding while still allowing BMPRIA and ActRII/ActRIIB to bind.

The BMP7/Noggin complex identified two key Noggin residues responsible for its ligand binding: Leu46, and Ile218. Noggin's Ile218 positions

itself in the hydrophobic pocket formed by BMP7 residues Ile57, Phe117, and Val123 while Noggin's Leu46 is inserted into a hydrophobic pocket formed by Leu115, Leu125, and Ala58 of BMP7 (11).

The residues that form the hydrophobic pocket for Noggin's Ile218 do not significantly differ between BMP7 and AB204 (Ile33, Tyr92, and Ile98). However, in the case of the hydrophobic pocket for Noggin's Leu46, Leu125 of BMP7 is replaced by the positively-charged Lys100 of AB204, which likely disrupts productive positioning of the Noggin's Leu46 in this hydrophobic pocket, thus resulting in significantly diminished Noggin binding to AB204 (Figure 3-8).

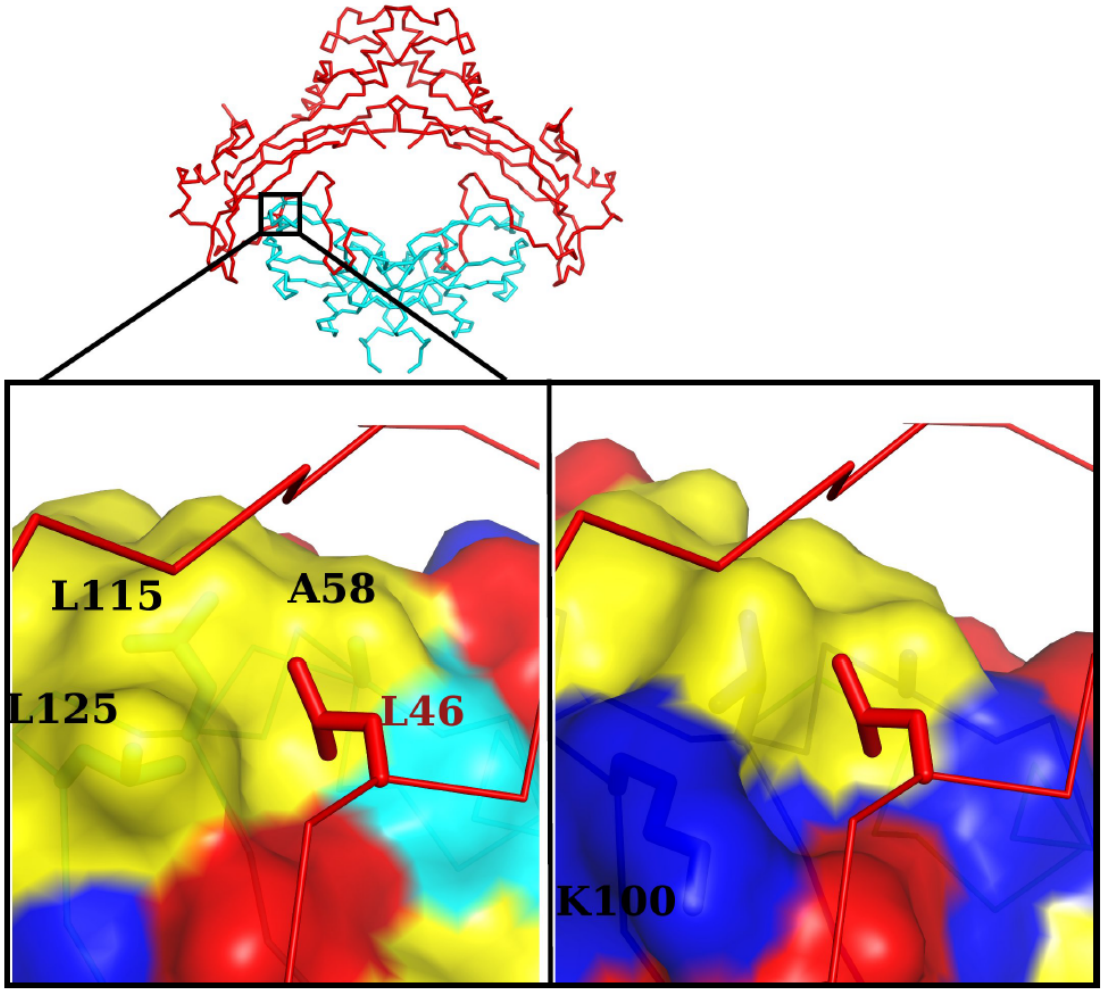

Figure 3-8: Key residues responsible for AB204's insensitivity to Noggin. Top image: BMP7 (cyan)/Noggin (red) complex. The key region of the BMP7/Noggin interface is boxed. Bottom left: close-up of this region showing Noggin's key residue Leu46 placed in the hydrophobic pocket on BMP7 created by its Ala58, Leu115, and Leu125 residues. Bottom right: same region, with BMP2 replaced by AB204 showing the effect of the substitution of BMP7's hydrophobic Leu125 residue with the charged AB204's Lys100 residue, which destroys the hydrophobic pocket. The surfaces are colored as follows: hydrophobic regions are depicted in yellow, polar and negatively charged regions are depicted in red, positively charged regions are depicted in blue, and neutral regions are depicted in cyan.

Despite the same structural fold between AB204 and BMP2, AB204 exhibits osteogenic activity significantly stronger than BMP2 both in vitro and in vivo. This improvement of the signaling output could likely be due to one or

a combination of the following properties: (1) AB204 possesses the complete Activin A type II receptor-binding epitope, which endows it with ~100-fold increased affinity to the type II receptor compared with BMP2's affinity, (2) AB204's decreased affinity for BMPRIA, and (3) Noggin's inability to downregulate AB204.

The structures of AB208 and AB204 have shown the power of the RASCH system to produce chimeras that are able to mimic the parental ligand and confer novel properties. Furthermore, these structures have provided valuable insight into the structural features that allow AB204 to achieve such enhanced levels of osteogenesis.

This chapter in part is currently being prepared for submission for publication of the material. Yoon BH, Esquivies L, Ahn C, Ye SK, Kwiatkowski W, Choe S. "A Noggin-insensitive Activin/BMP2 chimera, AB204, strongly accelerates osteogenic differentiation of preosteoblastic MC3T3-E1 cells and heals non-union bone defects in mice". The dissertation author was a co-author of this paper.

References

1. Pangas S, Woodruff T (2001) Production and purification of recombinant human inhibin and activin. *The Journal of Endocrinology* **172**: 199-210.

2. Harrison C, Gray P, Fischer W, Donaldson C, Choe S, Vale W (2004) An activin mutant with disrupted ALK4 binding blocks signaling via type II receptors. *The Journal of biological chemistry* **279**: 28036-28044.

3. Allendorph G, Read J, Kawakami Y, Kelbe J, Isaacs M, Choe S (2011) Designer TGFb Superfamily Ligands with Diversified Functionality. *PLoS ONE* **6**:e26402.

4. Peran M, Ruiz S, Kwiatkowski W, Marchal J, Yang S, Aranega A, Choe S, Izpisua Belmonte J (2013) Activin/BMP2 chimeric ligands direct adipose-derived stem cells to chondrogenic differentiation. *Stem cell research* **10**: 464-476.

5. Kabsch W (2010) XDS*. Acta Crystallogr D Biol Crystallogr* **66(Pt 2)**: 125–132.

6. Emsley P, Lohkamp B, Scott WG, Cowtan K (2010) Features and development of Coot. *Acta Crstallogr D Biol Crsytallogr* **66(Pt 4):** 486-501.

7. Murshudov GN, Vagin AA, Dodson EJ (1997) Refinement of macromolecular structures by the maximum-likelihood method. *Acta Crystallogr. D. Biol. Crystallogr.* **53(Pt 3):** 240-255.

8. The PyMOL Molecular Graphics System, Version 1.3 Schrödinger, LLC.

9. Kraulis PJ (1991) MOLSCRIPT: A Program to Produce Both Detailed and Schematic Plots of Protein Structures. *Journal of Applied Crystallography* **24**: 946-950.

10. Allendorph GP, Vale WW, Choe S (2006) Structure of the ternary signaling complex of a TGF-b family member. *Proc. Natl. Acad. Sci. USA* **103**: 7643-7648.

11. Groppe J, Greenwald J, Wiater E, Rodriguez-Leon J, Economides A, Kwiatkowski W, Affolter M, Vale W, Izpisua Belmonte J, Choe S (2002) Structural basis of BMP signalling inhibition by the cystine knot protein Noggin. *Nature* **420**: 636–642.

12. Greenwald J, Vega ME, Allendorph GP, Fischer WH, Vale W, Choe S (2004) A Flexible Activin Explains the Membrane-Dependent Cooperative Assembly of TGF-β Family Receptors. *Molecular Cell* **15**:485-489.

Chapter 4. Structural studies of GDF6 and GDF7, two tenogenic members of the TGF-β superfamily

Introduction

GDF6 and GDF7 (also referred to as BMP13 and BMP12, respectively), are members of a subset of proteins from the BMP subfamily of TGF-β ligands that have been found, in addition with GDF5, to induce cartilage, tendon, and ligaments *in vivo*, as opposed to having osteogenic properties like other members of the BMP family (1). It has been observed that treating tendon ruptures with these ligands increases levels of tenogenic marker Thbs4, and that these ligands are capable of inducing and accelerating tendon repair (2). Furthermore, it has been shown that GDF6 and GDF7 can induce ligament differentiation in fibroblasts from the medial collateral (MCL) and anterior cruciate (ACL) ligaments (3).

The mechanism of how these ligands are capable of inducing and repairing tendon and other ligaments is unknown. Studies have noted that GDF6 and GDF7 do not mediate increased expression levels of tenogenic marker Thbs4 via the Smad 1/5/8 signaling pathway commonly used by osteogenic BMPs, despite the fact that these ligands share receptors with osteogenic BMP counterparts and have similar affinities to these receptors (1).

Therefore, in order to determine the structural features that might be responsible for discrimination between osteo-, teno-, and chondrogenic properties of BMP ligands the structures of GDF6 and GDF7 were solved and compared to known structures of BMPs.

GDF6 CRYSTALLIZATION

GDF6 was resuspended in water to a concentration of 10 mg/ml. 192 crystallization conditions were screened using the Mosquito crystallization robot (ttp labtech, Cambridge, MA). This screen yielded 5 conditions that exhibited crystals in various crystal systems (Figure 4-1). These conditions were optimized in order to improve crystal size and quality.

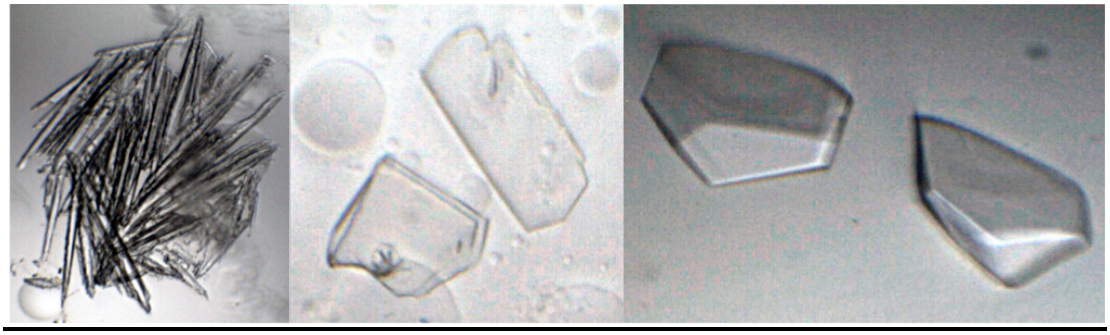

Figure 4-1: GDF6 crystals obtained from crystal condition optimization.

Fifty crystals were harvested and shot at SSRL beamline 11-1. 10% Glycerol was used as cryoprotectant. These crystals diffracted to resolutions between 4.1-2.5 Å. The crystal with the highest resolution was grown using the hanging drop vapor diffusion method at 15 ^{o}C in 0.2 M NH_4 Acetate, 0.1 M Na Citrate pH 5.6, 30% MPD. Data were processed using XDS software (4) and the structure was solved in the $P2_12_12_1$ space group using molecular replacement with BMP2 as a model. Model building was done in COOT version 0.6.2 (5). Refinement of the structure was completed using REFMAC, version 5.5.0109 (6) to R and R_{free} values of 0.21 and 0.24, respectively. All structure figures were generated using PyMOL (7). Processing and refinement statistics are presented in table 4-1.

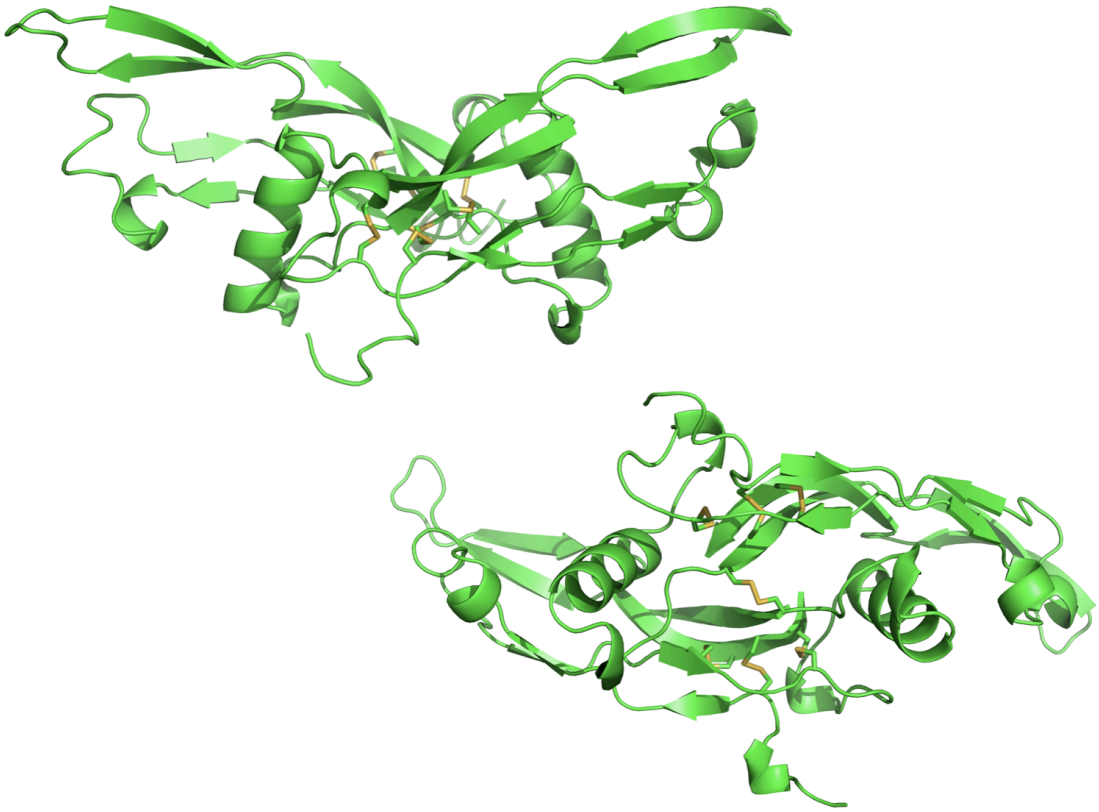

Figure 4-2: Structure of GDF6. Top: front view, bottom: 90° rotation.

Table 4-1: Data processing and refinement statistics for GDF6. Numbers in parentheses correspond to the highest resolution shell.

GDF6 X-ray Data Collection and Refinement Statistics	
Observed Reflections	106,870
Unique Reflections	16,617
Resolution Range (Å)	55.27-2.27 (2.39-2.33)
Mean (I/σ)	24.01 (3.1)
Completeness (%)	98.7 (98)
R_{merge}	0.060 (0.55)
R_{cryst}	0.21
R_{free}	0.24

The structure of GDF6 (Figure 4-2) shares its overall dimer architecture with other TGFβ ligands. The mature GDF6 ligand has three intra-disulfide bonds (Cys19/Cys86, Cys49/Cys118, and Cys53/Cys119) and one inter-disulfide bond between the Cys85 of each monomer. These disulfide bonds

along with the alpha helix (residues Asn65-Met76) comprise the core of the protein. Four anti-parallel β-sheets extending outward from the core give the ligand a spread-wing shape, which is characteristic of all TGF-β family members.

GDF7 Crystallization

Initial attempts at resuspending GDF7 in water were unsuccessful due to the fact that this protein will only solubilize to the concentrations required for crystallization at an acidic pH. Thus, the protein was resuspended in 10 mM Na Acetate pH 4.4 to a concentration of 11.6 mg/ml. 192 crystallization conditions were screened using the Mosquito robot, and four conditions were subsequently optimized. The crystal with the best diffraction pattern had a needle morphology, and was grown using the hanging drop vapor diffusion method at 15 °C in 0.1 M Na Citrate pH 6.2, 0.1 M Na Cacodylate pH 6.5, 25% Isopropanol (Figure 4-3).

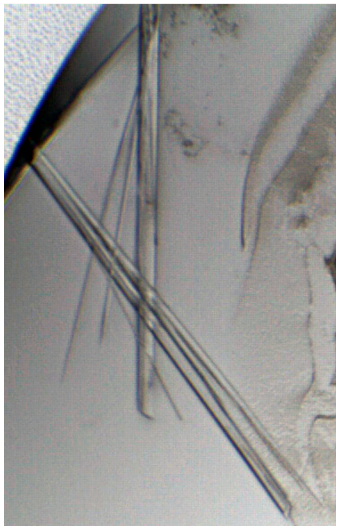

Figure 4-3: Needle GDF7 crystals obtained after optimization and used for x-ray analysis.

One full dataset was collected in house using a Rigaku MicroMax 007HF x-ray generator (Rigaku, Tokyo, Japan) to a resolution of 3.5 Å. The structure was solved in the $P2_111$ space group using GDF5 as a model. Data were processed using XDS software (4). Model building was done in COOT version 0.6.2 (5). Refinement of the structure was completed using REFMAC, version 5.5.0109 (6) to R and R_{free} values of 0.28 and 0.26, respectively. All structure figures were generated using PyMOL (7). Processing and refinement statistics are presented in table 4-2.

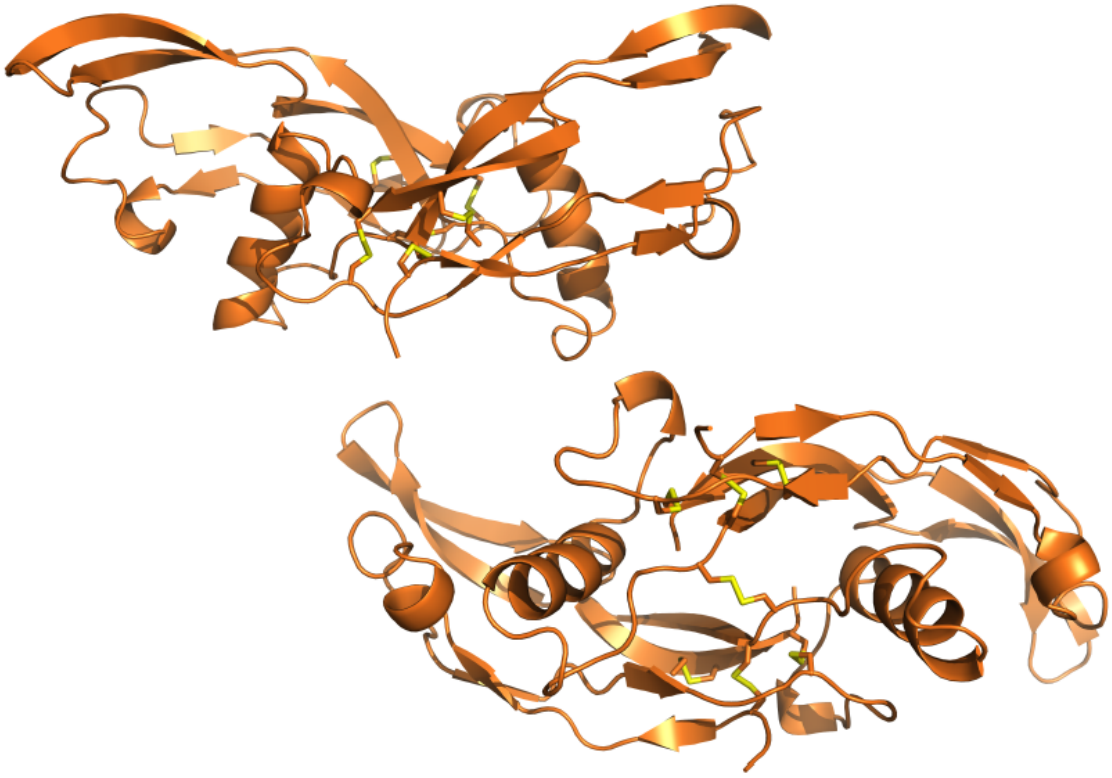

Figure 4-4: Structure of GDF7. Top: front view Bottom: 90° rotation.

Table 4-2: Data processing and refinement statistics for GDF7. Numbers in parentheses correspond to the highest resolution shell.

GDF7 X-ray Data Collection and Refinement Statistics	
Observed Reflections	25,301
Unique Reflections	7,262
Resolution Range (Å)	64.51-3.5 (3.68-3.5)
Mean (I/σ)	6.9 (2.9)
Completeness (%)	98.4 (98.5)
R_{merge}	0.0161 (0.376)
R_{cryst}	0.276
R_{free}	0.259

The structure of GDF7 (Figure 4-4) is quite similar to that of GDF6. Following the architecture of a mature TGF-β ligand, GDF7 exhibits a core composed of an α-helix (Asn74-Met85), a cysteine knot constituted by three intra-disulfide bonds (Cys29/Cys95, Cys58/C127, and C62/C129), and one inter-disulfide bond between the Cys94 of each monomer. Extending outwards from this core are four β sheets in a spread-wing configuration, which gives this ligand the “butterfly” appearance that characterizes TGF-β ligands.

Discussion

The structures of GDF6 and GDF7 have been solved to a resolution of 2.3 Å and 3.5 Å, respectively. Both ligands conserve the canonical TGF-β "spread-wing" configuration, with a flexibility that is intermediate between the NB250 (rigid, BMP-like) and AB208 (flexible, Activin-like) chimeras previously analyzed.

Comparing these structures with BMP2 indicate that both GDF6 and GDF7 share structural similarity with this ligand. Alignment of GDF6 and GDF7 with BMP2 yield RMSD values of .802 (Figure 4-5A) and 0.753 (Figure 4-5B) respectively. Furthermore, these alignments indicate that both GDF6 and GDF7 share a BMP-like fold with other members of the BMP family.

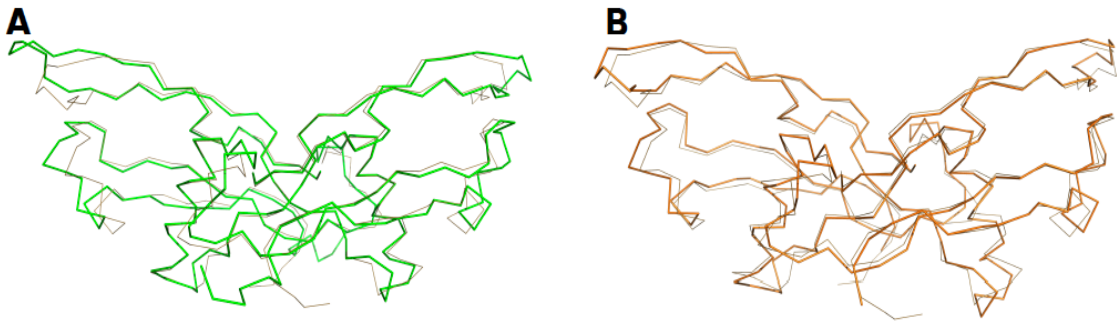

Figure 4-5: C_α alignment of A) GDF6 (green) and BMP2 (sand), and B) GDF7 (orange) and BMP2 (sand).

GDF5, GDF6, and GDF7 share 82% of their sequence (1). Thus, it is highly likely that these three ligands are structurally similar, and have type I and type II binding epitopes that resemble each other.

Using the previously solved structure of GDF5 (8), it was confirmed that all three ligands share a high structural similarity. Cα alignment of GDF5 with

GDF6 and GDF7 yielded RMSD values of 0.561 (Figure 4-6A) and 0.874 (Figure 4-6B), respectively. Interestingly, the highest discrepancy was found between GDF6 and GDF7, which exhibits a RMSD of 1.02 (Figure 4-6C). For all alignments, the main differences can be found in finger 2 of the dimers, which suggests receptor binding selectivity among these three ligands.

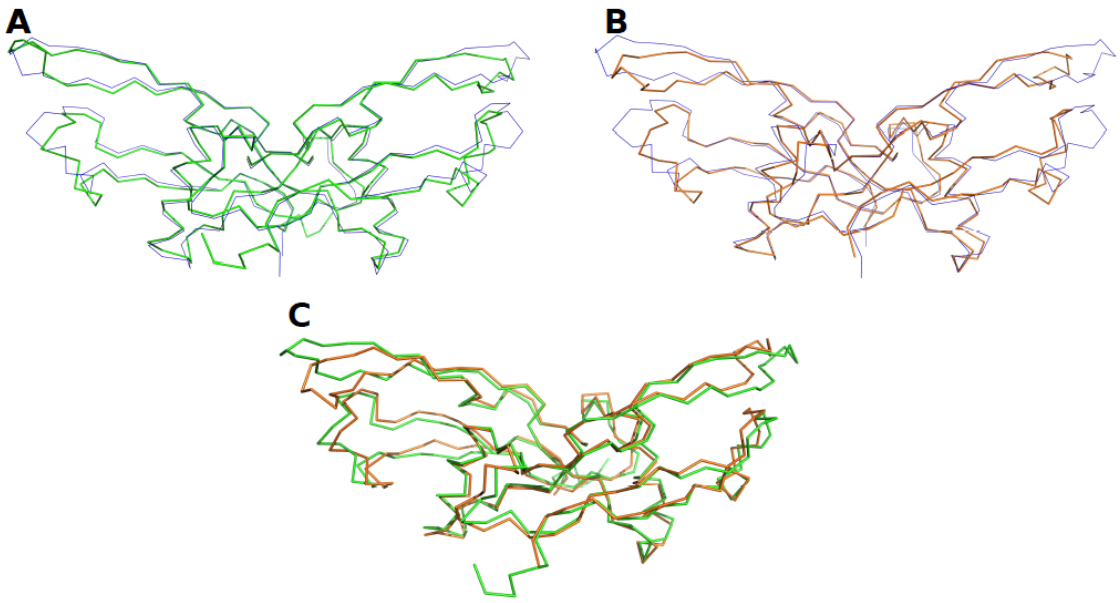

Figure 4-6: C_α alignment of A) GDF6 (green) and GDF5 (blue), B) GDF7 (orange) and GDF5 (blue), and C) GDF6 (green) and GDF7 (orange).

Binding affinity studies have shown that GDF5, 6 and 7 have a preference for binding type I receptor BMPRIB (9,1). Curiously, GDF5 has been shown to have a significantly higher preference for this receptor over BMPRIA, whereas GDF6 and 7's affinity for BMPRIA and B is approximately equal. Nickel et al determined that GDF5's predilection for BMPRIB can be abolished by mutating the Arg57 residue located in the type I receptor binding

pocket of this ligand. When this residue is changed to an Ala, affinity for BMPRIA is restored to levels seen in GDF6 and 7.

Nickel et al's proposed model for the GDF5-BMPRIA complex (in which GDF5 has the R57A mutation) (9) was used in an effort to gain some insight into GDF6 and 7's binding mechanism to type I receptors, as well as to determine whether there is a structural change in GDF5 caused by the Arg57Ala substitution that is mimicked by GDF6 or 7 in order to bind BMPRIA with high affinity. Structural and sequence analysis of the GDF5, 6, and 7 type I binding epitopes indicate that all the residues involved in the formation of this binding pocket (with the exception of the mutated Arg57) are shared by all three ligands. Furthermore, the type I receptor binding pocket of GDF5R57A does not exhibit any overt structural differences with the type I binding pockets of GDF6 and 7 (Figure 4-7). Therefore, based on sequence and structural analyses it can be determined that the differences in receptor preference between GDF5 and GDF6 and 7 cannot be attributed to any significant structural changes in GDF5's binding pocket.

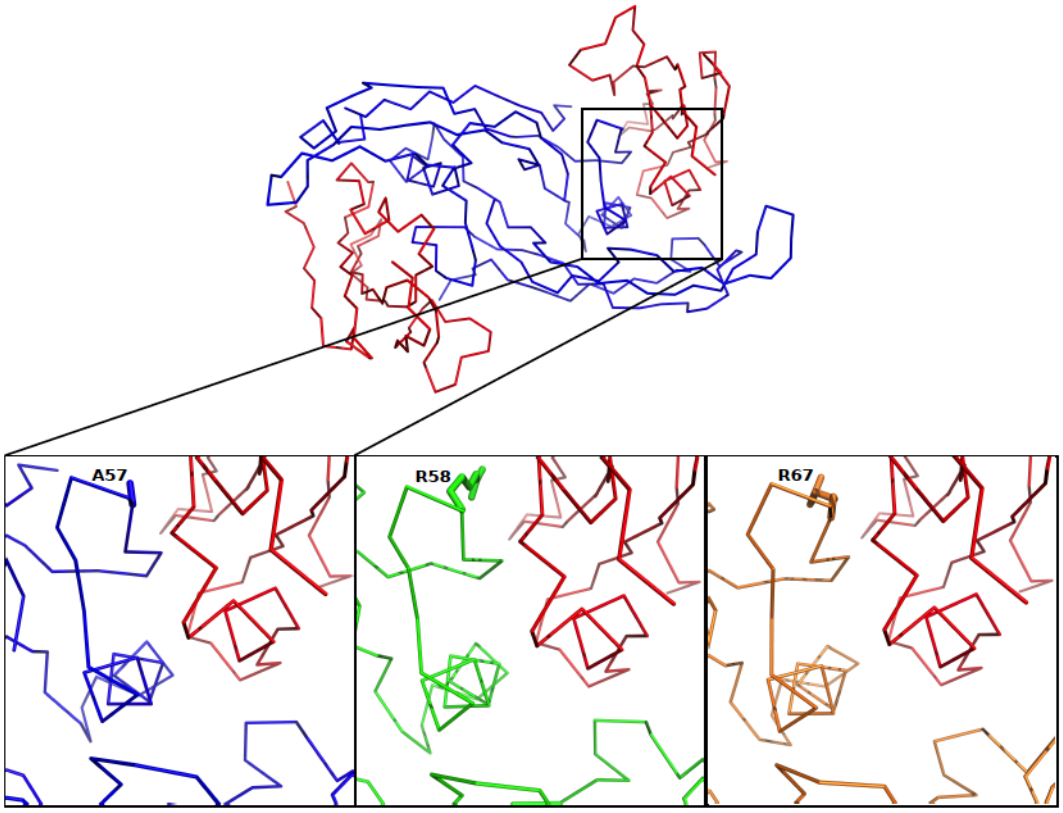

Figure 4-7: BMPRIA interface with GDF5R57A (blue), GDF6 (green), and GDF7 (orange).

Previous studies have shown that the ligand trap Noggin can block GDF6 and GDF7 signaling (10,11). Structural analysis of GDF6 and GDF7 has provided valuable insight into how Noggin interacts with these ligands, and reveals that this ligand trap binds GDF6 and GDF7 in the same manner as it binds other BMPs.

Noggin binds its ligands using their type I and type II receptor binding epitopes. Furthermore, it has been discovered that four Noggin residues play a key role in its ability to bind BMP7 (12). BMP7 residues Trp52, Trp55, Val87, Y128, and Met131 form a hydrophobic pocket into which Noggin Pro35 inserts

itself, mimicking type I BMPRIA receptor binding. Additionally, functional studies discovered that three Noggin residues (Leu46, Glu48, and Ile218) play a key role in the proper binding of this ligand trap (12). Leu46 and Ile218 interact with the BMP7 type II receptor binding site by inserting themselves into hydrophobic pockets formed by BMP7 residues Ile57, Phe117, and Val123 (in the case of I218), and Ala58, Leu115, and Leu125 (in the case of Leu46) (12).

By superimposing GDF6 and GDF7 over the BMP7/Noggin complex, it can be observed that all three ligands conserve the binding epitopes required for Noggin binding, albeit with some changes in the residue composition of the hydrophobic pockets exploited by Noggin.

The type I receptor binding epitope in GDF6 and GDF7 shares its amino acid composition with BMP7 with the exception of residue Val87 (BMP7 numbering), which is equivalent to residues Ile69 and Ile78, respectively. This amino acid change should not perturb the binding pocket, given that both Val and Ile are hydrophobic residues (Figure 4-8) and should still allow for the proper placement of the Pro35 residue.

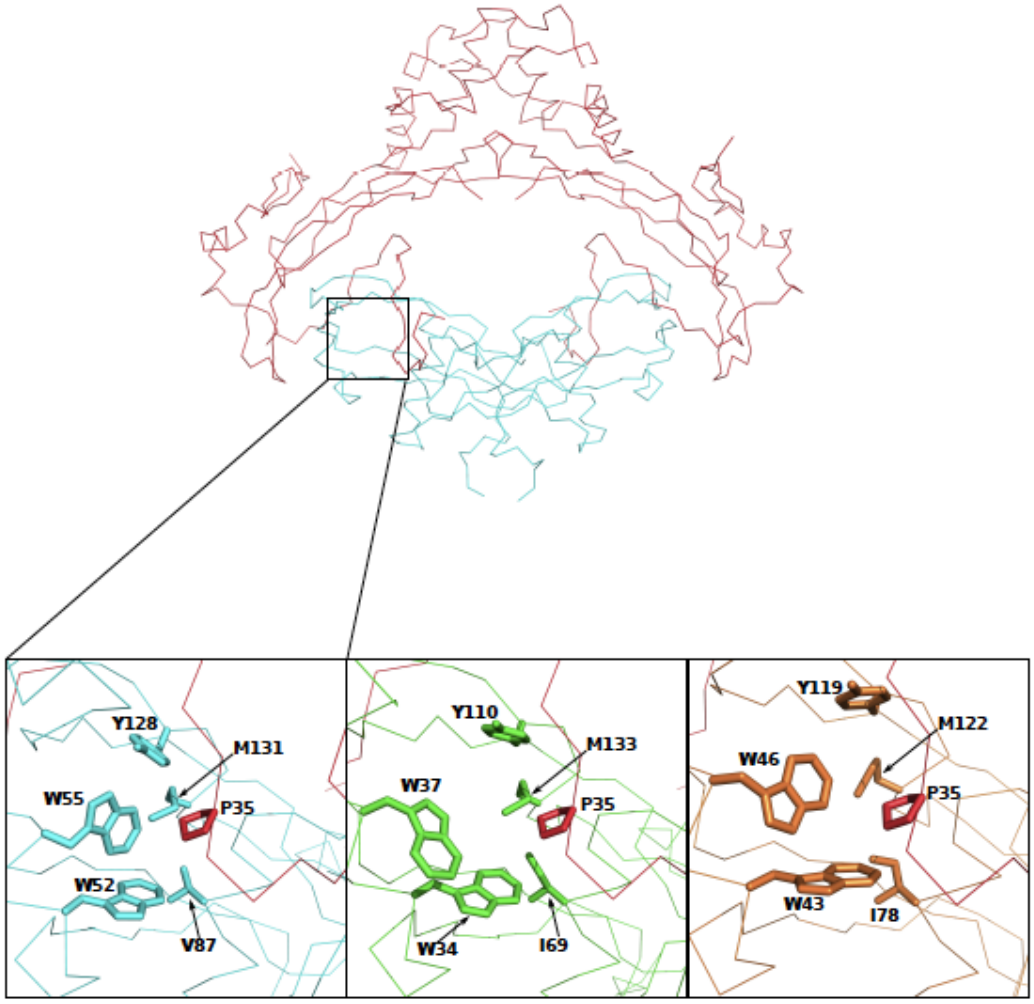

Figure 4-8: Noggin Pro35 binding pocket in BMP7 (cyan), GDF6 (green), and GDF7 (orange).

The binding pockets for residues Leu46 and Ile218 have also suffered changes in their amino acid composition. Sequence analyses of GDF6 and GDF7 show that residue Phe117 in the Ile218 binding pocket has been replaced by Tyr99 in GDF6 (GDF6 numbering) and Ile108 (GDF7 numbering) in GDF7. Furthermore, residue Leu125 in BMP7 has been replaced by a Tyr in

the Leu46 binding pocket for both GDF ligands (Tyr107 in GDF6 and Tyr116 in GDF7).

While the Tyr and Ile substitutions in the Ile218 binding pocket are considered to be conservative substitutions, the Tyr substitution in the Leu46 binding pocket raises the possibility of interactions between the GDF6/7 binding pocket and Noggin not seen in the BMP7/Noggin complex. The presence of a Tyr residue in the pocket in place of a Leu (Figure 4-9) suggests the possibility of the formation of a salt bridge or a hydrogen bond between this residue and the Asp residue adjacent to Leu46. This new interaction would confer GDF6 and 7 a higher affinity for Noggin compared to BMP7. Previous studies using quantitative competition assays have indeed shown that Noggin can bind GDF6 with higher affinity than BMP7, and that BMP7 is unable to outcompete GDF6 for Noggin (10).

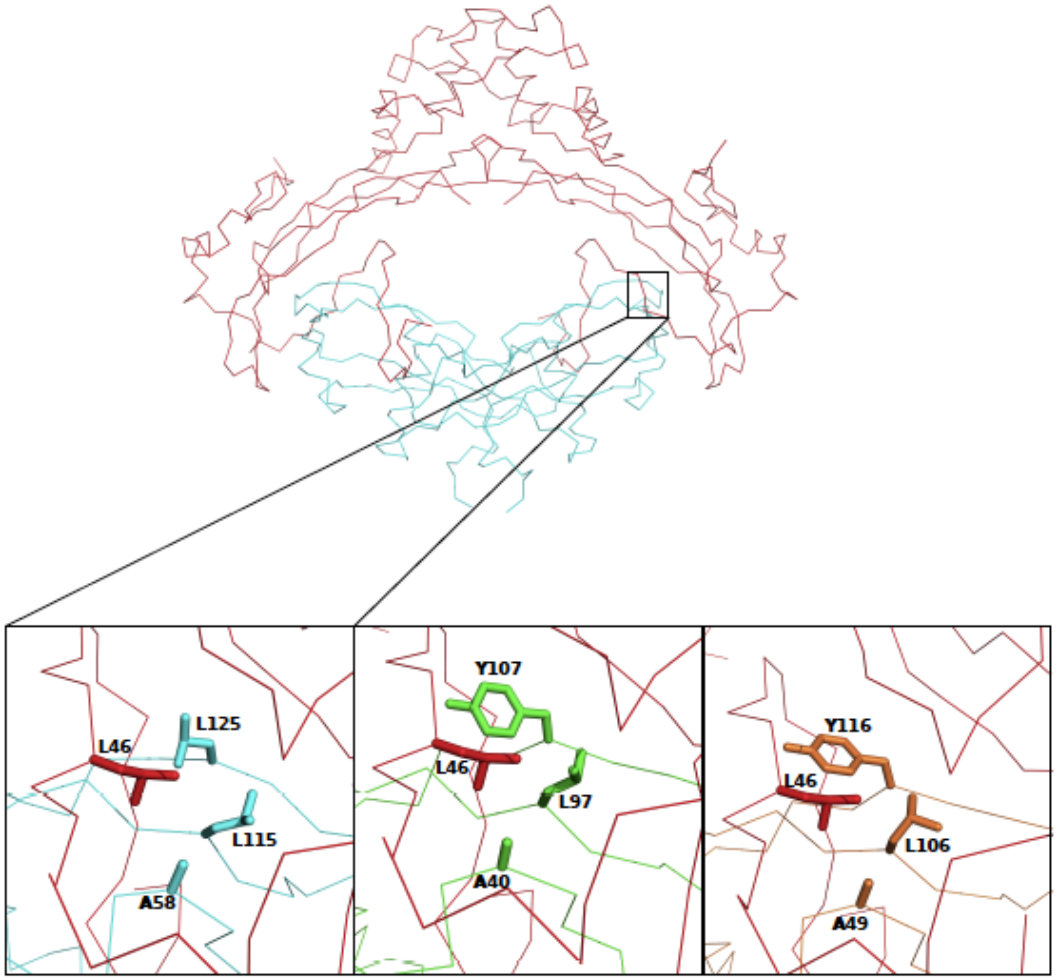

Figure 4-9: Noggin Leu46 binding pocket in BMP7 (cyan), GDF6 (green), and GDF7 (orange).

The determination and analysis of the structures of GDF6 and GDF7 have provided valuable insight into the binding mechanisms of these ligands and their affinity for their receptors and inhibitors. Both ligands exhibit the characteristic BMP ligand architecture, and share a close structural homology with GDF5. Furthermore, structural analyses suggest that GDF6 and 7 share their type I and II receptor binding epitopes with GDF5, and thus are able to bind the same receptors (BMPRIA, ActRII/IIB).

Additionally, the structures elucidated in this study provide a possible explanation for GDF6's ability to bind Noggin with a higher affinity than BMP7, and suggest that GDF7 binds Noggin with an affinity closer to that of GDF6.

References

1. Berasi SP, Varadarajan U, Archambault J, Cain M, Souza TA, Abouzeid A, Li J, Brown CT, Dorner AJ, Seeherman HJ, Jelinsky SA (2011) Divergent activities of osteogenic BMP2, and tenogenic BMP12 and BMP13 independent of receptor binding affinities. *Growth Factors* **29**: 128-139.

2. Jelinsky S, Archambault J, Li L, Seeherman H (2010) Tendon-selective genes identified from rat and human musculoskeletal tissues. *Journal of orthopaedic research : official publication of the Orthopaedic Research Society* **28**: 289–297.

3. Haddad-Weber M, Prager P, Kunz M, Seefried L, Jakob F, Murray M, Evans C, Nöth U, Steinert A (2010) BMP12 and BMP13 gene transfer induce ligamentogenic differentiation in mesenchymal progenitor and anterior cruciate ligament cells. *Cytotherapy* **12**: 505–513.

4. Kabsch W (2010) XDS. *Acta Crystallogr D Biol Crystallogr* **66(Pt 2)**: 125–132.

5. Emsley P, Lohkamp B, Scott WG, Cowtan K (2010) Features and development of Coot. *Acta Crstallogr D Biol Crsytallogr* **66(Pt 4):** 486-501.

6. Murshudov GN, Vagin AA, Dodson EJ (1997) Refinement of macromolecular structures by the maximum-likelihood method. *Acta Crystallogr. D. Biol. Crystallogr.* **53(Pt 3):** 240-255.

7. The PyMOL Molecular Graphics System, Version 1.3 Schrödinger, LLC.

8. Schreuder H, Liesum A, Pohl J, Kruse M, Koyama M (2005) Crystal structure of recombinant human growth and differentiation factor 5: evidence for interaction of the type I and type II receptor-binding sites. *Biochemica and Biophysical Communications* **329**: 1076–1086.

9. Nickel J, Kotzsch A, Sebald W, Mueller T (2005) A single residue of GDF-5 defines binding specificity to BMP receptor IB. Journal of molecular biology **349**: 933–947.

10. Chang C, Hemmati-Brivanlou A (1999) Xenopus GDF6, a new antagonist of noggin and a partner of BMPs. *Development* **126**: 3347–3357.

11. Lee K, Mendelsohn M, Jessell T (1998) Neuronal patterning by BMPs: a requirement for GDF7 in the generation of a discrete class of commissural interneurons in the mouse spinal cord. *Genes & development* **12**: 3394–3407.

12. Groppe J, Greenwald J, Wiater E, Rodriguez-Leon J, Economides A, Kwiatkowski W, Affolter M, Vale W, Izpisua Belmonte J, Choe S (2002) Structural basis of BMP signalling inhibition by the cystine knot protein Noggin. *Nature* **420**: 636–642.

Chapter 5. Discussion and Future Directions

TGF-β ligands have been shown to play a crucial role in numerous aspects of development. Their ability to influence a wide range of biological processes given their limited number of signaling receptors highlights the importance of studying how these signaling complexes are assembled and the usefulness of investigating the structural nuances that make these ligands elicit such diverse biological responses. The goal of this work was to focus on the study of TGF-β ligands involved in the development of the musculoskeletal system. The crystal structures presented in this work have contributed to the understanding of the underlying mechanisms responsible for ligand receptor selection. Additionally, these structures have helped put forth an explanation of the novel properties observed in some of the chimeric ligands studied.

Previous structural studies of TGF-β ligands (1,3) have allowed the development of novel techniques that have produced a number of chimeric proteins able to mimic their parental ligands as well chimeras that exhibit novel properties. The RASCH method for producing ligands (1) has been an invaluable tool in the study of members of the TGF-β superfamily that are difficult to produce in the amounts required for structural and functional studies, such as Nodal and Activin. Furthermore, the RASCH strategy offers the opportunity to create ligands with novel properties, with the implication that these ligands could be used for treatments of a variety of ailments. However, in order to exploit this strategy to its full potential, structural studies are necessary in order to properly guide the design of future chimeras.

The structures of NB250, AB208, and AB204 are the first reported structures of protein ligands that contain structural elements and functional properties from Nodal and BMP2 (in the case of NB250), and Activin and BMP2 (in the case of AB208 and AB204). These structural models highlight how the responses elicited by these ligands are controlled at the amino acid level, as the structures presented suggest that the enhanced properties observed on these chimeras could be attributed to small changes in their receptor binding epitopes. These changes allow these ligands to either modify or establish novel affinities for receptors involved in the signaling pathways associated with their new biological functions. Additionally, the models elucidated have provided a structural basis for explaining the insensitivity of some of these chimeric ligands to ligand traps, which is a property that can exponentially increase the chimeric ligands' potency. Furthermore, the functional studies of the NB2 chimeras propose a novel role for Nodal in chondrogenesis. This finding is substantiated by the structure of NB250, which suggests that Nodal may have a BMP2-like structure.

After comparing the NB250 and AB208 structures and assessing their flexibility, it can be seen that they lie on opposite sides of the spectrum. While the AB208 structure suggests that it is a very flexible ligand, NB250 exhibits the rigidity of BMP2. The flexibility of these ligands may play a very important role in the formation of their respective signaling complexes, since ligand flexibility may determine the positioning of its receptors. Furthermore, ligand

flexibility may also play a role in the observed chondrogenic properties of the NB2 chimeras.

It has been shown that some of the AB2 and NB2 chimeric ligands have properties that can be used as therapeutics to treat ailments such as bone fractures and cartilage regeneration. Therefore, the elucidation of structures such as NB250 and AB204 are vital to determine the structural features that dictate these ligands' chondrogenic and osteogenic properties, as well as to shed light on the underlying signaling mechanisms employed by these ligands to elicit their biological effects. These structural features can then be exploited and preserved in the development of future therapeutic agents.

The structure of NB250 represents the first structure of a Nodal/BMP2 ligand, while the structure of AB204 is the first structure of an Activin A/BMP2 ligand that exhibits increased levels of osteogenesis. Nonetheless, there are several NB2 and AB2 ligands that are also worthy of structural studies, such as the NB260 and AB235 chimeras. NB260 exhibits higher chondrogenic activity than BMP2 and NB250, yet it has one less BMP2 segment than NB250. AB235, a chimera based on AB208 that exhibits sensitivity to Noggin, has been shown to induce chondrogenesis at levels higher than those observed for AB204 (5). Based on these observations, the structures of NB260 and AB235 can yield important insight into how NB2 and AB2 chimeras can induce chondrogenesis and osteogenesis at levels higher than those observed for BMP2. Furthermore, additional NB2 and AB2 structures would aid in determining whether there are significant structural differences among

chimeric ligands of the same family, or if they follow a general structure with small changes in some areas of the protein.

The elucidation of the structures of NB250 or AB208 with their type I, type II receptors, and/or Cripto will prove very valuable in determining whether these chimeras are assembling similar signaling complexes as those observed for BMP2 and Activin. The structure of NB250 is quite similar to that of BMP2, and the same can be said for AB208 and Activin A. Combining this with the fact that NB250 and AB208 appear to be indistinguishable from Nodal and Activin, respectively, in their signaling (3), it can be concluded that NB250 and AB208 are likely structural as well as a functional equivalents of Nodal and Activin. NB250's rigidity should facilitate structural studies of relevant complexes including the NB250/Cripto/ActRII/Alk4 complex, and the elucidation of this complex together with the Activin/Cripto/ActRII/Alk4 complex will be instrumental to understanding how the signaling of Nodal and Activin, which share the same set of type I and type II receptors, is regulated by co-receptor Cripto.

Members of the GDF family have been shown to play a role in tenogenesis, among other biological functions. Prior to this work, the structure of only one member of this subset of BMPs (GDF5) was known (4). The elucidation of the GDF6 and GDF7 structures has shown that these ligands share a BMP-like structure with their osteogenic counterparts. Furthermore, these structures provide valuable insight into the structural elements shared with BMPs that make them susceptible to Noggin inhibition. Lastly, these

structures, in conjunction with the RASCH strategy, could be used to develop chimeras with novel properties, such as enhanced tenogenic activity.

Structural studies of GDF6 and GDF7 have shown that they share the same type II receptor with BMP2, yet they elicit very different developmental pathways. Mutagenesis studies that would replace key residues in GDF6 and GDF7 receptor binding epitopes for those found in BMP2, that is, making the GDF ligands more “BMP2-like”, will aid in determining whether the tenogenic response activated by GDF6 and GDF7 can be attributed to a single residue or a group of residues in their binding epitopes.

The structural insights obtained from NB250, AB208, AB204, GDF6 and GDF7 warrant the continued structural and functional studies of the AB2 and NB2 family of chimeras, as well as the development of new chimeric ligand families derived from GDF6, GDF7, Activin, and Nodal. Additionally, it would be interesting to develop additional chimeric families involving more than two parental ligands. Surely, these chimeras hold the promise of novel therapeutic agents and will play a vital role in solving the complexities of TGF-β signalling.

References

1. Greenwald J, Vega M, Allendorph G, Fischer W, Vale W, Choe S (2004) A flexible activin explains the membrane-dependent cooperative assembly of TGF-beta family receptors. *Molecular cell* 15:485–489.

2. Allendorph G, Vale W, Choe S (2006) Structure of the ternary signaling complex of a TGF-beta superfamily member. *Proc Natl Acad Sci USA* **103**:7643–7648.

3. Allendorph G, Read J, Kawakami Y, Kelber J, Isaacs M, Choe S (2010) Designer TGFβ superfamily ligands with diversified functionality. *PLoS ONE* **6**:e26402

4. Schreuder H, Liesum A, Pohl J, Kruse M, Koyama M (2005) Crystal structure of recombinant human growth and differentiation factor 5: evidence for interaction of the type I and type II receptor-binding sites. *Biochemical and biophysical research communications* **329**:1076–1086

5. Peran M, Ruiz S, Kwiatkowski W, Marchal J, Yang S-L, Aranega A, Choe S, Izpisua Belmonte J (2013) Activin/BMP2 chimeric ligands direct adipose-derived stem cells to chondrogenic differentiation. *Stem cell research* **10**:464–476.

Chapter 6. Materials and Methods

NB2/AB2 Chimera Expression and Purification

To create the NB2 chimera library, the mature domains of human Nodal and human BMP2 were divided into 6 segments. Twelve Nodal/BMP2 primers corresponding to each segment were ordered from Integrated DNA Technologies (Coralville, Iowa). An overlapping PCR strategy was used to combine the various segments together to generate a full-length PCR fragment of each chimera. In order to create overlapping regions for PCR, residues A77 and L95 in Nodal were changed to Valine. The constructs were cloned into pET21A vector (EMD Biosciences Darmstadt, Germany) and propagated in Nova Blue cells (EMD Biosciences Darmstadt, Germany). Final expression constructs were confirmed by DNA sequencing.

All NB2 chimeras were expressed in *Escherichia coli* as inclusion bodies and isolated, purified, and refolded using a modified protocol (1). The refolded ligands were initially purified using Hi-trap Heparin sulfate (GE Healthcare) and a Sodium Chloride gradient. Fractions containing the refolded ligand were submitted to a second round of purification using a C4 reverse phase column (GraceVydac). The protein was eluted using an acetonitrile gradient. Nodal was purchased from R&D Systems.

AB2 chimeras were produced in the same manner as the NB2 chimeras, substituting Nodal for Activin A.

Luciferase, phospho-SMAD2 Assays and ASCs cell culture

Luciferase and phospho-SMAD2 assays were performed as previously described (2). Human mesenchymal stem cells were derived from the adipose tissue of the subcutaneous abdomen of a 37-year-old Caucasian female (lot number 9061601.12, PromoCell, Heidelberg, Germany). Cells were cultured in “growing medium”: high glucose Dulbecco's modified Eagle's medium (DMEM, Invitrogen) with 10% fetal bovine serum and 1% penicillin/streptomycin (Invitrogen).

Induction of monolayer expanded cells toward chondrocytes

Human ASCs were induced to chondrogenic phenotype as previously described (3). Briefly, cells were seeded at 30-40% of confluence in 12 or 24-well plates. Control cells were grown in “incomplete chondrogenic medium”: DMEM–high glucose (Invitrogen) supplemented with 10% fetal bovine serum and 1% ITS+Premix (Collaborative Biomedical–Becton Dickinson, Bedford, MA), plus 1% penicillin–streptomycin (Invitrogen). In addition, 50 mg/mL of l-ascorbic acid 2-phosphate (Sigma-Aldrich) was freshly added at each media exchange. To direct chondrogenic differentiation, cells were cultured in “chondrogenic medium”: incomplete chondrogenic medium containing 10 ng/ml of the Nodal ligand. Media was changed every other day. Cells were cultured in chondrogenic media for 2, 4 and 6 weeks depending on the experiment. Complete chondrogenic medium with 10 ng/ml of BMP2, known to be capable of chondrogenesis, was used as positive control.

Chondrogenic differentiation in cell pellet culture

Cells were grown on 12-well plates in chondrogenic medium. Upon reaching confluence, the cell monolayer detached itself from the plate and took the form of a crumpled ball. Control cells grown in incomplete chondrogenic medium did not detach spontaneously from the plastic and, therefore, the monolayer was manually separated using a sterile tip. The pellets were transferred to 15-ml conical tubes and incubated with loosened caps at 37 °C and 5% CO2. Media was exchanged every other day for the duration of the experiment, and the tubes were gently agitated to avoid the adherence of the pellet to the tube walls.

RNA isolation and real-time PCR analysis

Total cellular RNA was isolated using Trizol Reagent (Invitrogen) according to the manufacturer's recommendations. 2µgs of DNAse1 (Invitrogen) treated total RNA was used for cDNA synthesis using the SuperScript II Reverse Transcriptase kit for RT-PCR (Invitrogen). Real-time PCR was performed using the SYBR-Green PCR Master mix (Applied Biosystems). Sequences of primers were 5´GGACTCATGACCACAGTCCAT GCC3´ and 5´TCAGGGATGACCTTGCCCACAG3´ for GAPDH; 5´AGGA TGGCTTCCACCAGTGC3´ and 5´TGCGTAAAAGACCTCACCCTCC3´ for Aggrecan (ACN); 5´GAGACAGCATGACGCCGAG3´ and 5´GCGGATGCTCT CAATCTGGT3´ for type II Collagen (COL2A1); 5´ACTCCGAGACGTGGA CATC3´ and 5´TGTAGGTGACCTGGCCGTG3´ for Sox9 (SOX9). The levels of expression of the respective genes were normalized to corresponding

GAPDH values and are shown as fold change relative to the value of the control sample. All the samples were done in triplicate.

Cell monolayer and cell pellet processing

For immunocytochemistry analysis, monolayer expanded cells were processed. Monolayer expanded cells were washed thrice in PBS and fixed with 4% paraformaldehyde for 20 min at room temperature.

In vivo assays

Chick embryos were explanted and grown in vitro as described (4). RCAS-Nodal retroviral stocks were produced as described (4) and used to infect, by air pressure, the right side of Hensen's node in developing chick embryos. Beads were soaked in Nodal-like NB250 compound and similarly applied locally on the right side of Hensen's node. Embryos were processed for whole mount *Pitx2 in situ hybridization* as previously described (4) or fixed in paraformaldehyde for heart looping visualization.

Fluorescence Microscopy

Briefly, after fixation, cells and sections were blocked and permeabilized for 1hr at 37º C with 5% BSA/5% appropriate serum/1X PBS with 0.1% Triton X100. Subsequently, cells and sections were incubated with the indicated primary antibody overnight at 4º C. The cells and sections were then washed thrice with 1X PBS and incubated for 2hr at 37º C with the respective secondary antibody. Cells and sections were washed thrice with 1X PBS; DAPI (0.5µg/ml in PBS) was added to the last wash. Cells were mounted with aqueous mounting media before analysis.

Primary antibody used was anti-type II Collagen antibody (mouse monoclonal antibody (ab3092), Abcam, Cambridge, MA). Alexa Fluor 568 or 488 (Neomarkers) were used as secondary antibodies. The localizations of the proteins were observed with a Leica TCS SP2 AOBS confocal or Nikon E-800 microscope.

Surface Plasmon Resonance (BIAcore) Affinity Studies

The affinity of NB250 to ActRII-ECD was measured using a Biacore 3000 (GE Healthcare). Using primary amine coupling, the receptor ECD was immobilized on a CM5 chip independently using flow cell 2. No protein was immobilized on flow cell 1 as a negative control. For kinetic analysis, all tests were performed in duplicate using a minimum of five concentrations, plus a zero concentration. Binding data was analyzed with BIAevaluation software ver. 4.1 (GE Healthcare) and fit using a global 1:1 Langmuir binding with mass transfer model.

References

1. Groppe J et al (1998) Biochemical and Biophysical Characterization of Refolded Drosophila DPP, a Homolog of Bone Morphogenetic Proteins 2 and 4. *The Journal of Biological Chemistry* **273**: 29052-29065.

2. Kelber JA, Shani G, Booker EC, Vale WW, Gray PC (2008) Cripto Is a Noncompetitive Activin Antagonist That Forms Analogous Signaling Complexes with Activin and Nodal. *J Biol Chem* **283**: 4490-4500.

3. Estes BT, Diekman BO, Gimble JM, Guilak F (2010) Isolation of adipose-derived stem cells and their induction to a chondrogenic phenotype. *Nat Protoc* **5**: 1294-1311.

4. Ryan AK, Blumberg B, Rodriguez-Esteban C, Yonei-Tamura S, Tamura K, Tsukui T, de la Peña J, Sabbagh W, Greenwald J, Choe S, Norris DP, Robertson EJ, Evans RM, Rosenfeld MG, Izpisua Belmonte JC (1998) Pitx2 determines left-right asymmetry of internal organs in vertebrates. *Nature* **394**: 545-551.